

**THE REPUBLIC OF TURKEY
BAHCESEHIR UNIVERSITY**

**DENDRITIC SPINE SEGMENTATION USING
ACTIVE CONTOUR WITH SHAPE PRIOR**

Master's Thesis

CEMAL AKARSU

ISTANBUL, 2012

**THE REPUBLIC OF TURKEY
BAHCESEHIR UNIVERSITY**

**GRADUATE SCHOOL OF NATURAL AND APPLIED
SCIENCES
ELECTRICAL AND ELECTRONICS ENGINEERING
PROGRAM**

**DENDRITIC SPINE SEGMENTATION USING
ACTIVE CONTOUR WITH SHAPE PRIOR**

Master's Thesis

CEMAL AKARSU

THESIS ADVISOR: ASSIST. PROF. DR. DEVRİM ÜNAY

ISTANBUL, 2012

**THE REPUBLIC OF TURKEY
BAHCESEHIR UNIVERSITY**

**GRADUATE SCHOOL OF NATURAL AND APPLIED SCIENCES
ELECTRICAL AND ELECTRONICS ENGINEERING PROGRAM**

Name of the thesis: Dendritic Spine Segmentation Using Active Contour with Shape Prior

Name/Last Name of the Student: Cemal Akarsu

Date of the Defense of Thesis: 08 June 2012

The thesis has been approved by the Graduate School of Natural and Applied Sciences.

Assoc. Prof. Dr. , Tunç BOZBURA
Graduate School Director
Signature

I certify that this thesis meets all the requirements as a thesis for the degree of Master of Science.

Assoc. Prof. Dr., M. S. Ufuk TÜRELİ
Program Coordinator
Signature

This is to certify that we have read this thesis and we find it fully adequate in scope, quality and content, as a thesis for the degree of Master of Science.

Examining Committee Members _____

Signature _____

Thesis Supervisor
Assist. Prof. Dr., Devrim ÜNAY

Member
Assoc.Prof. Dr., Çiğdem EROĞLU ERDEM

Member
Assoc. Prof. Dr., Gözde ÜNAL

ACKNOWLEDGEMENTS

First and foremost I would like to thank my advisor Assist. Prof. Dr. Devrim Ünay for his invaluable guidance and support throughout my study. I very much appreciate his suggestions, detailed reviews, invaluable advices and life lessons. I particularly want to thank him for his confidence and belief in me during my study. He has been a great mentor and I feel privileged to be his student.

I would like to thank all members of the Neuronal Structure and Function Laboratory in Champalimaud Centre for the Unknown, Lisbon, Portugal; Dr. Inbal Israely, Ali Özgür Argunşah, Yazmın Ramiro-Cortés and Anna F. Hobbiss for their great ideas, support and the images they provided for our study.

I am sincerely grateful to my thesis committee members, Assoc.Prof. Dr. Çiğdem Erođlu Erdem and Assoc. Prof. Dr. Gzde Ünal, for their invaluable feedback.

I also thank Melih Soydemir, Tevfik Zafer Özcan and Serkan Kangel who have been greatly supportive during my study. I also would like to thank Kbra alıřkan who was always there for me and provided me with endless motivation.

I would also like to express my deepest gratitude for my beloved family, Ayřen and Hamdi Akarsu, who always believed in me, and always tried their best to make things easier for me.

Finally I would like to acknowledge Bahcesehir University for supporting me throughout my graduate education.

Cemal Akarsu

ABSTRACT

DENDRITIC SPINE SEGMENTATION USING ACTIVE CONTOUR WITH SHAPE PRIOR

Cemal Akarsu

Electrical and Electronics Engineering Program

Thesis Supervisor: Assist. Prof. Dr. Devrim Ünay

June 2012, 58 Pages

Dendritic spine analysis is a popular topic in Neuroscience, since the morphological and statistical (e.g. quantity and density) properties of dendritic spines play a role in the learning process, and can be used for understanding the reasons of mental disorders like Alzheimer's. Advancements in the related imaging technology has lead to vast amount of dendritic spine images that need to be analyzed and interpreted by the experts. But manual analysis of these images is a difficult and time-consuming task. Therefore, automated tools are required, which should detect, segment, and quantify statistical properties of dendritic spines, such as length and volume.

To this end, a collaborative effort on creating a software tool for automated analysis of dendritic spines is being carried out at Bahçeşehir University. This thesis is focused on the automated segmentation part of this collaborative effort. For accurate segmentation of dendritic spines, application of the Active Contour with Shape Prior method is proposed. Performance of the proposed method is evaluated on an expert-annotated dataset, and compared with the accuracy of two other methods; Global Thresholding and Active Contour.

Results are presented both visually and quantitatively using the Dice overlap measure. Results show that applying the Active Contour with Shape Prior method leads to more accurate segmentations than Global Thresholding and Active Contour methods. Furthermore, accuracy and robustness of the proposed method is increased if it is applied on Otsu thresholded images instead of the original grayscale versions.

Keywords: Dendritic Spine, Segmentation, Active Contour with Shape Prior, Otsu Thresholding, Two-Photon Microscopy.

ÖZET

DENDRİTİK OMURGALARIN ŞEKİL BİLGİSİ KULLANAN AKTİF KONTURLAR İLE SEGMENTASYONU

Cemal Akarsu

Elektrik - Elektronik Mühendisliği Programı

Tez Danışmanı: Yrd. Doç. Dr. Devrim Ünay

Haziran 2012, 58 Sayfa

Dendritik omurga analizi Sinirbilimi'nin popüler konularından birisidir. Bunun nedeni bu yapıların morfolojik ve istatistiksel özelliklerinin öğrenme sürecinde etkili olması ve bu özelliklerin incelenmesinin *Alzheimer* gibi hastalıkların sebeplerini bulmada yardımcı olabileceği olmasıdır. Bu konuya olan yoğun ilgiye ve görüntüleme teknolojilerindeki ilerlemelere bağlı olarak önemli miktarda dendritik omurga resmi birikmiştir ve bunların hepsi uzmanlar tarafından görsel olarak analiz edilmeyi beklemektedir. Ancak bu resimlerin görsel analizi hem zor hem de vakit alan bir işlemdir. Bu nedenle otomatik araçlara gerek duyulmaktadır. Bu araçlar dendritik omurgaları tespit etmeli, uygun bir şekilde bölütlemeli ve hacim, uzunluk gibi istatistiksel özelliklerini ölçmelidir.

Bu tezde çalışmaları devam etmekte olan otomatik analiz aracının, otomatik bölütleme kısmına odaklanılmıştır ve dendritik omurganın doğru bir şekilde bölütlenmesi için şekil bilgisi kullanan aktif çevrit metodunun kullanılması önerilmiştir. Bu tezde bu metodun *MATLAB* ortamında gerçekleştirilmesi kullanılmıştır. Sonuçlar, global eşikleme ve aktif çevrit metodlarının sonuçlarıyla karşılaştırılmıştır.

Bölütleme sonuçları hem görsel olarak hem de *Dice* skoru üzerinden sayısal bir şekilde verilmiştir. Bu sonuçlara göre şekil bilgisi kullanan aktif çevrit metodu, global eşikleme ve aktif çevrit metodlarına göre daha gerçekçi sonuçlar vermektedir. Ayrıca bu yöntemi gri tonlanmış resimler yerine *Otsu* eşikleme uygulanmış resimlere uygulamak metodun doğruluğunu ve sağlamlığını arttırmaktadır.

Anahtar Kelimeler: Dendritik Omurga, Segmentasyon, Şekil Bilgisi Kullanan Aktif Kontur, Otsu Eşikleme, Çift-Foton Mikroskop.

CONTENTS

TABLES	vii
FIGURES	viii
ABBREVIATIONS	xi
SYMBOLS	xii
1. INTRODUCTION	1
2. LITERATURE SURVEY	5
3. METHODS	16
3.1 IMAGE ACQUISITION	16
3.2 REGION OF INTEREST (ROI) SELECTION	17
3.3 DENOISING	17
3.4 GLOBAL THRESHOLDING BASED SEGMENTATION	18
3.5 ACTIVE CONTOUR BASED SEGMENTATION	18
3.6 ACTIVE CONTOUR WITH SHAPE PRIOR BASED SEGMENTATION .	24
4. RESULTS	34
4.1 SELECTION OF MEDIAN FILTER SIZE	35
4.2 RESULTS OF GLOBAL THRESHOLDING BASED SEGMENTATION ..	36
4.3 RESULTS OF ACTIVE CONTOUR BASED SEGMENTATION	37
4.4 RESULTS OF ACTIVE CONTOUR WITH SHAPE PRIOR BASED	39
SEGMENTATION	39
4.5 EFFECT OF ROI SELECTION	44
5. DISCUSSIONS AND RESULTS	49
5.1 RESULTS	49
5.2 FUTURE WORKS	52
REFERENCES	53

TABLES

Table 2.1: Summary of literature survey.	14
Table 4.1: Dice scores obtained in the early stages of the study for Active Contour with Shape Prior method.	35
Table 4.2: Dice scores obtained in the final stage of the study for Active Contour with Shape Prior method.	35
Table 4.3: Segmentation results for spine number 1-12 (S denotes Spine).	43
Table 4.4: Dendritic spine segmentation results on the overall data set.	44

FIGURES

Figure 1.1: An image from our database showing a dendrite and the spines.....	1
Figure 1.2: Diagram of two photon microscope.	2
Figure 2.1: Comparison of the method given in Zhang et al. (2007) with manual analysis.....	7
Figure 2.2: Exemplary result of Bai et al.'s method.	8
Figure 2.3: Comparison of manual analysis and the results of NeuronIQ.	9
Figure 2.4: 3D reconstruction of a neuron image realized using the method given at Janoos et al. (2009).	10
Figure 2.5: Results given in the study of Choy et al. (2010).	11
Figure 3.1: Image of hippocampus and its regions.	16
Figure 3.2: Image on the left is original maximum intensity projection of dendrite image and the image on the right is the median filtered of this image.	17
Figure 3.3: Graphics of regularized H_ϵ and δ_ϵ	22
Figure 3.4: Training set.....	24
Figure 3.5: Mean shape obtained from the training set (Figure 3.4).....	25
Figure 4.1: Exemplary segmentation with Otsu Thresholding of Spine 1 (Dice score=0.54). Blue corresponds manual segmentation and red represents automated segmentation.....	36
Figure 4.2: Exemplary segmentation with Otsu Thresholding of Spine 8 (Dice score=0.91). Blue corresponds manual segmentation and red represents automated segmentation.....	37

Figure 4.3: Exemplary segmentation with Active Contour of Spine 1 (Dice score=0.8). Blue corresponds manual segmentation and red represents automated segmentation.	38
Figure 4.4: Exemplary segmentation with Active Contour of Spine 5 (Dice score=0.57). Blue corresponds manual segmentation and red represents automated segmentation.	39
Figure 4.5: Exemplary segmentation using Active Contour with Shape Prior on Grayscale image of Spine 1 (Dice score=0.84). Blue corresponds manual segmentation and red represents automated segmentation.	40
Figure 4.6: Exemplary segmentation using Active Contour with Shape Prior on Grayscale image of Spine 4 (Dice score=0.46). Blue corresponds manual segmentation and red represents automated segmentation.	41
Figure 4.7: Exemplary segmentation using Active Contour with Shape Prior on Otsu thresholded image of Spine 4 (Dice score=0.89). Blue corresponds manual segmentation and red represents automated segmentation.	42
Figure 4.8: Dice scores of Active Contour with Shape Prior.....	43
Figure 4.9: Effect of the horizontal shift of the manually selected ROI on the segmentation accuracy. Horizontal axis represents the percentage shift relative to the horizontal size of the ROI (“-” values show left-shift); whereas, vertical axis corresponds to the Dice score. Blue markers represent the mean values, while the corresponding error bars depict standard deviations.....	45

Figure 4.10: Effect of vertical shift of manually selected ROI to the segmentation accuracy. Horizontal axis represents the percentage shift relative to the vertical size of the ROI (“-” values show up-shift); whereas, vertical axis corresponds to the Dice score. Blue markers represent the mean values, while the corresponding error bars depict standard deviations.	46
Figure 4.11: Effect of ROI size on the segmentation accuracy.....	47
Figure 4.12: Effect of ROI rotation on the segmentation accuracy. Blue markers represent the mean result of segmentation in the range of ± 15 to the angle found with semi-automated method. Red marker refers to the result of the expert’s manual ROI selection.	48

ABBREVIATIONS

μ EPSC	:	Micro-Excitatory Postsynaptic Current
ROI	:	Region of Interest
MIP	:	Maximum Intensity Projection
2D	:	Two Dimensional
3D	:	Three Dimensional
LDA	:	Linear Discriminate Analysis
SNR	:	Signal-to-Noise Ratio
CADMOS	:	Curvilinear-based Automatic Detection and Measurement Method
SDF	:	Signed Distance Function
PCA	:	Principal Component Analysis
MSN	:	Medium-sized Spiny Neuron

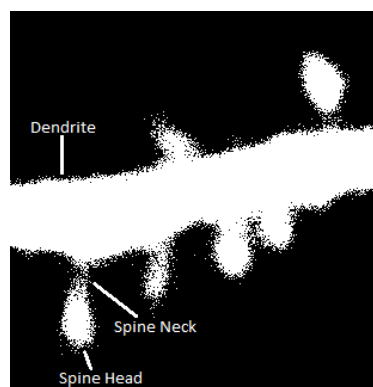
SYMBOLS

Energy minimization function	: F
Evolving curve in Active Contour Method	: C, \emptyset
Average intensity value in curve C	: u_i
Average intensity value outside curve C	: u_o
Constant values in F	: $c_1, c_2, \mu, \nu, \lambda_1, \lambda_2, \beta_s, \beta_b, \beta_r$
Heaviside function	: H
One-dimensional Dirac measure	: δ_0
Inside of the active contour	: ω
Eigen coefficients vector	: \mathbf{x}_{pca}
Geometric transformation vector	: \mathbf{x}_T
Shape function	: $\hat{\emptyset}$
Dice score function	: D

1. INTRODUCTION

Neuron is a cell that processes and transmits information by electrical and chemical signaling, and their basic cellular organizations are similar to other cells. Their main difference from other cells is their specialization for communication occurred between cells. This specialization appears in their morphology, in the placement of the membrane components that are related with electrical signaling and in the complexity of the synaptic contacts between neurons. Nerve cells have branches called as dendrite for targeting electrical inputs from synapses of other cells (Purves 2008). Dendrites are connected to short protrusions with a thin neck and these are defined as spine. Dendritic spines found in higher animals and in some insects are discovered in the 19th century and carefully investigated at 20th century (Ramon 1995; Greenough 1988; Coss 1985; Leiss 2009). Pyramidal neurons in the cortex, medium spiny neurons in the basal ganglia and Purkinje cells in the cerebellum are some example cells that contain dendritic spines. An exemplary image of a dendrite and the spines connected to this dendrite can be seen in Figure 1.1.

Figure 1.1: An image from our database showing a dendrite and the spines.

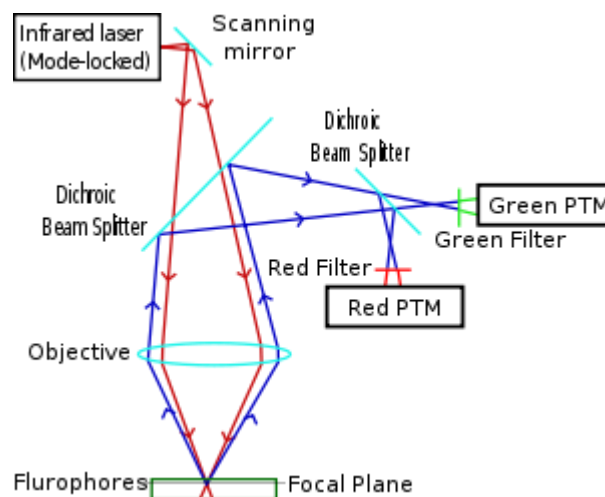


Dendritic spines were considered as stable structures before the monitoring of living tissues with fluorescence microscopes, such as two-photon excitation microscopy. This advancement in the imaging of cells showed that dendritic spines are changing shapes in their lifespan (Yuste and Bonhoeffer 2001). Advances in the field of imaging has made

possible to investigate the correlation between neuronal structures and their function at the level of dendritic spines (Harvey et al. 2007; Govindarajan et al. 2011; Jun-ichi et al. 2008). For instance, the μ EPSCs evoked at a spine has an effect on the volume of dendritic spine and activity induced spatio-temporal interactions of dendritic spines is used for determining the direction of the plasticity at a dendritic branch which can be a factor on some neurodegenerative diseases such as Fragile X syndrome (Bear et al. 2004).

In fluorescence microscopy a molecule absorbs a photon with an energy that triggers the emission of another photon with a longer wavelength from this molecule. The absorbed photon in this interaction is usually in the ultraviolet range; whereas, the emitted photon results with a light in visible range (Valeur 2001). Two-photon excitation microscopy introduced by Denk et al. (1990) is also based on this concept. In this imaging technique the necessary energy for the excitation of the molecule is acquired from the absorption of two photons with lower energy instead of absorption of one photon with higher energy. In Figure 1.2 a diagram of two photon microscope can be seen.

Figure 1.2: Diagram of two photon microscope.



Source: Two-photon excitation microscopy. [online] http://en.wikipedia.org/wiki/Two-photon_excitation_microscopy. [accessed 17 July 2012].

As it can be seen from the Figure 1.2, infrared laser beam from a femtosecond laser is focused on an objective. At that part selection of laser is crucial. A femtosecond laser with high flux of excitation is necessary to increase the low probability of the near-simultaneous absorption of two photons (Göppert-Mayer, 1931). Then, the fluorescence

excited from the sample is collected by photomultiplier tube which is a high-sensitivity detector. This observed light intensity coming from one focal point creates one pixel in the resulting image. By scanning this focal point throughout a desired region the complete image can be created.

Using lower energy and longer wavelength infrared light as the source of two photon absorption will result with deeper tissue imaging up to one millimeter and reduced photochemical destruction of a fluorophore which is the eventual result of light exposure from fluorescent molecules. Thanks to these properties of two-photon excitation microscopy researchers can observe dendritic spines more deeply and longer times.

Researchers state that (i) morphological and statistical (such as quantity and density) properties of dendritic spines are crucial in understanding neurological disorders, and (ii) changes in the structure of dendritic spines may have an effect on learning process (Choy et al. 2010). The increase in the number of studies on neuronal structure at the level of dendritic spines has resulted with the collection of large amount of data that need to be analyzed. However manual analysis of these data sets is a tedious and time-consuming process that needs to be automated (Cheng et al. 2007). Prior art on such automated tools include solutions e.g. for detecting spines on a dendritic branch (Bai et al. 2007) or estimating spine volume (Zhang et al. 2010) that generally focus on only one aspect of the dendritic spine analysis problem.

Accordingly we work towards creating a software tool for dendritic spine analysis, and in this thesis we present a solution on a part of this problem: automated dendritic spine segmentation.

Prior art on automated analysis of dendritic spines includes segmentation approaches such as local adaptive thresholding (Cheng et al. 2007; Weaver et al. 2004; Rodriguez et al. 1997), global thresholding (Janoos et al. 2009) and watershed segmentation (Choy et al. 2010; Son et al. 2010). But these algorithms are mostly employed for spine detection, and therefore their results are mostly focused on the success of the detection process rather than segmentation. In this thesis, we propose the use of Active Contour with Shape Prior (Bresson et al. 2006) for segmentation of dendritic spines, and

compare its segmentation accuracy with respect to two different approaches: Global (Otsu) Thresholding and an Active Contour based approach.

In Section 2 of this thesis, literature survey will be given with a summary table and explanations of some studies from this table will be presented. In this part, studies will be compared based on the main parts of dendritic spine analysis; pre-processing, spine detection, spine segmentation and post-processing.

In Section 3, methods used in this thesis will be explained. Image acquisition, Region of Interest (ROI) and denoising steps will be briefly given at the beginning of this part. Then, methods applied for the segmentation of Dendritic Spines in this thesis, Global thresholding via Otsu thresholding method, Active Contour model proposed by Chan and Vese (2001) and Active Contour with Shape Prior method of Bresson (2006) will be explained in detail.

In Section 4, segmentation results obtained via methods explained in Section 3 will be presented separately. In Section 5, comparison of these results and comments on the overall status of the thesis in the light of these results will be discussed.

2. LITERATURE SURVEY

General overview on dendritic spine analysis is aimed to be given by explaining some studies in literature at this part. In Table 2.1, summary of a literature survey are presented in a comparative manner.

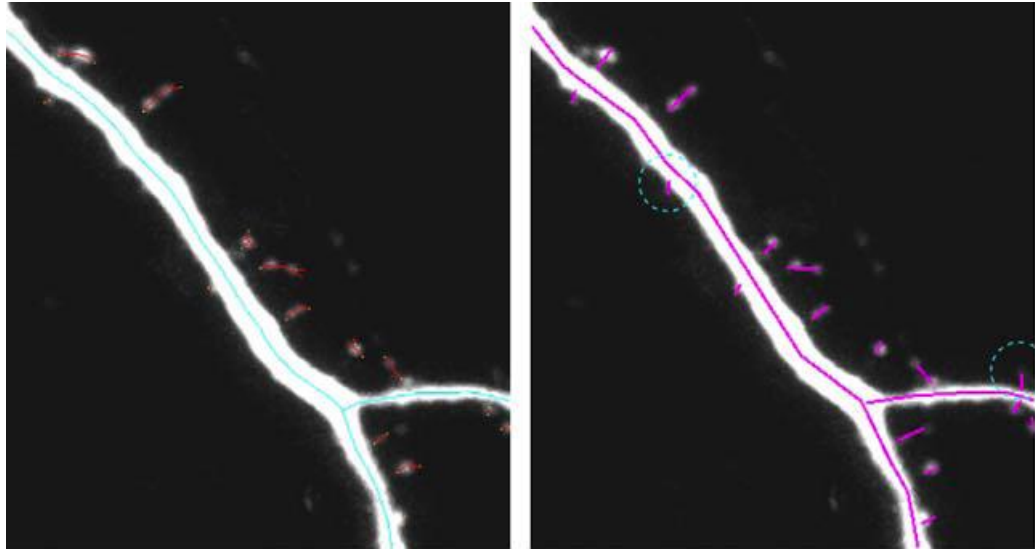
Paper written by Kasai et al. (2010) is crucial since it is a review paper summarizing new findings on dendritic spine structural dynamics and functional plasticity; and can be helpful to enlighten why there are several studies on this topic. In respect of this study, following results were obtained:

- i. Enlargement of the spines depends on protein synthesis, and according to the results structural plasticity is the main cellular mechanism for memory formation.
- ii. Volume of spines can show instantaneous growth or shrinkage, whereas average volume change of a spine population remains at zero which means volume of a spine population is in equilibrium and individual spines can be memory elements.
- iii. Smaller spines reflect greater activity-dependent structural changes. On the other hand, older spines follow the trend of being larger and having longer life expectancies. As a result, spine volume can give information about the history of a spine.
- iv. As a consequence of intrinsic fluctuations occurred on spine structure, some smaller spines can be eliminated that leads cleared space and recycled molecular resources in dendrite, which can be used in the generation of new spines.
- v. Memory content and strength is managed by activity-dependent plasticity, whereas they are rarely affected from instant fluctuations.
- vi. Clinical evidences showed that abnormally small and immature spines can cause problems on the accumulation of knowledge in the developmental period that can lead a deficit in general intelligence.

As it can be seen from the result stated by Kasai et al. (2010) volume, density and morphology of spine are related with learning and memory, and can be used in the studies of mental disorders. Therefore, dendritic spine image analysis is an important research area for neuroscientists. Some of these studies on dendritic spine analysis are summarized in the following part of this section.

In Zhang et al. (2007)'s study the spines are recognized as small variable-shaped objects that are attached (connected to the dendrite with a neck) or detached (not connected to the dendrite with a neck but close to it) to multiple dendritic backbones in 2D MIP (maximum intensity projection) images from two-photon laser scanning microscopy. As a preprocessing step median filtering is applied on the images for noise removal. The method proposed by Zhang et al. (2007) consists of two main parts; (a) multi-scale curvilinear structure detector algorithm that treats all dendritic structures (including spines) as curvilinear structures and extracts their center lines and boundaries by estimating the second order directional derivatives. As a result of this part, small shapes along dendrite backbone are detected. In the second part of this method (b) a Linear Discriminate Analysis (LDA) based approach is used to classify detected small shapes into two classes, namely protrusion or spine, since first part detects both valid and invalid regions as spine. In this part a training set that contains features of both spine and protrusions obtained from Zernike moments and geometric features of manually selected shapes from both classes is used to train the LDA classifier. For evaluation of the method proposed by authors, results are compared with manual measurements provided by experts in terms of backbone length, spine number, spine length and spine density. For instance, 241 spines were detected both manually and by automated method. 13 additional spines were detected only manually, whereas, automated tool detected 19 additional spines. In Figure 2.1, the image on the left is an exemplary result of this method; whereas, the image on the right is the result of manual analysis for the same dendrite. The spines circled in the manual analysis are removed by the automated method since they are classified as protrusions.

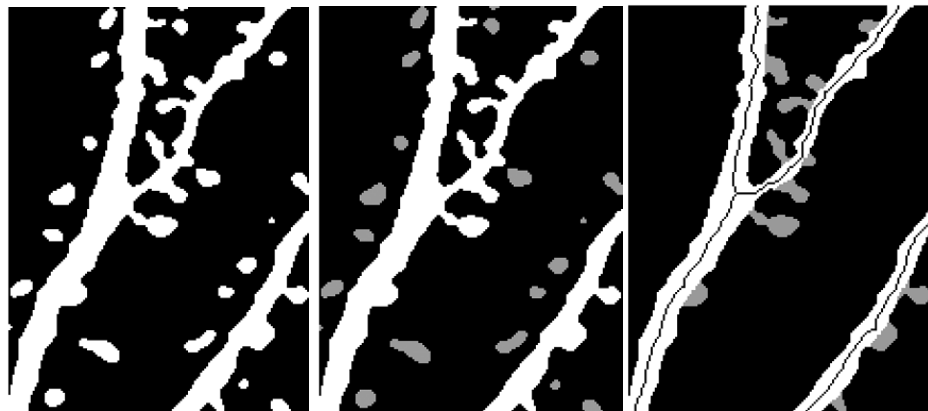
Figure 2.1: Comparison of the method given in Zhang et al. (2007) with manual analysis.



Bai et al. (2007) proposed another method for analysis of dendritic spine images taken with two-photon microscopy. This method is started with a preprocessing stage that consists of three different steps; (1) blind deconvolution algorithm for deblurring image stacks using the commercial software Autodeblur (AutoQuant Imaging, Watervliet, NY), (2) unsharp mask filtering to correct uneven image in intensity and (3) median filtering. Preprocessing step is followed by binarization of MIP image with a threshold value to separate the dendritic region from background. Spine segmentation on binary images is divided into two categories; (a) segmentation of detached spines and (b) segmentation of attached spines. For segmentation of detached spines a width-based criteria is used. According to this criterion, a region that has a larger area than a defined value is accepted as dendrite with attached spines and other parts in the binary image are isolated and these parts are defined as detached spines. Segmentation of attached spines starts with extraction of dendrite skeleton with a thinning algorithm and is followed with Bresenham's line algorithm (Hearn et al. 1996) which is used for extending the skeleton to the boundary of the connected region. In the extended skeleton image, each protruding branch length is measured and the branches with smaller length than a predefined value are defined as attached spines, while the remaining branches are assigned as dendritic branches which are neither attached nor detached dendritic spine. But the number of spines can be wrong as a result of false segmentation. Therefore, attached and detached spine decisions are refined according to some additional criteria

based on width and length. This method can be used for analysis of spine number, spine length and spine density. Results of this method were validated by comparison with manual results provided by experts, e.g. in an image set that contains 653 manually detected dendritic spines, and automated tool correctly detected 575 dendritic spines whereas it wrongly detected 90 and missed 78 dendritic spines. Figure 2.2 displays a binary image of a dendritic region (left), the detected detached spines labeled with gray color (middle), and the detached spines removed and the detected attached spines labeled with gray color (right).

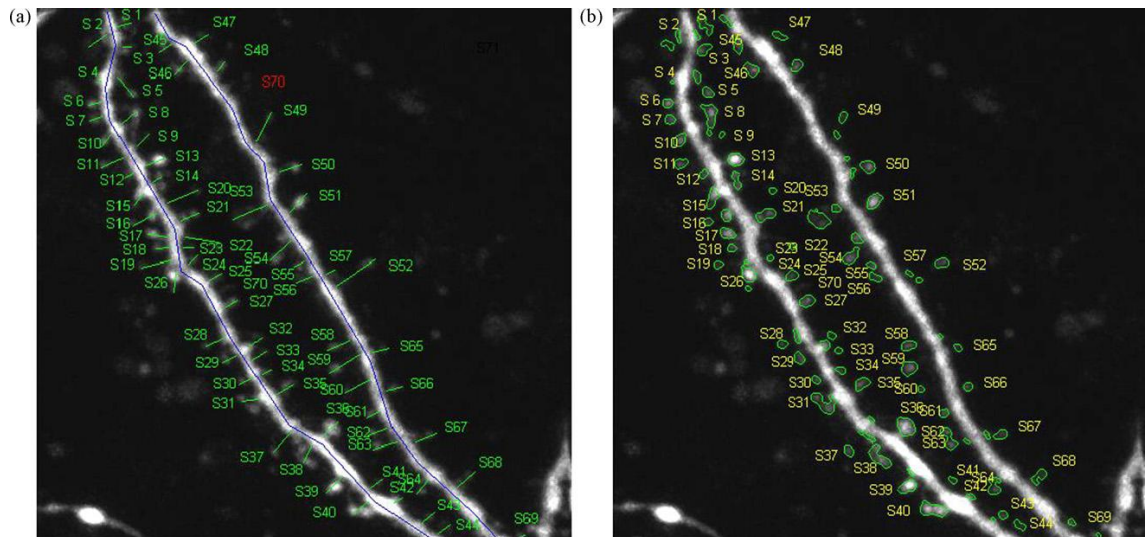
Figure 2.2: Exemplary result of Bai et al.'s method.



Cheng et al. (2007) provided a toolbox called NeuronIQ for analysis of dendritic spines as a result of their study. This study is also started with a preprocessing step for noise reduction via median filtering. After denoising, dendrite and spines need to be extracted from the background by adaptive thresholding. Binarization of the image is followed by backbone extraction with recursive trimming algorithm. Then, the backbone is dilated to eliminate the region that is not considered as potential spine area. By this way authors obtain a region that can potentially contain attached or detached spines. In the first part of detection process, detached spines are detected with a signal-to-noise ratio (SNR) based algorithm, which is applied on potential detached spines and if the result is higher than a threshold (obtained by clustering); this blob is detected as a detached spine. However, some non-spine blobs can be falsely detected as spine. This can be avoided by adding a term to SNR based algorithm that considers the 3D intensity properties of a spine. Authors stated that the resolution in z -direction is much lower compared with other directions and the intensity value of a non-spine blob between successive slices in z -direction is more stable whereas it changes obviously in dendritic spines. Therefore,

this new term searches for an obvious change between the neighbor slices of a dendrite in z-direction and if it finds, it marks this blob as detached spine. Otherwise, this blob defined as a non-spine region. In the second part of detection process attached spines are detected using medial axis-based attached spine detection algorithm. This algorithm consists of the following steps; backbone removal from medial axis, estimating local thickness of dendrite, marking candidate spines and eliminating others. Then, a final filtering applied on candidate spines according to area and edge criteria to eliminate false spines. Authors stated that some detached and attached spines can represent the same spine as a result of weak neck part of a spine. Therefore, a merging algorithm is suggested to correct the number of spines detected. In the final step of this study authors calculated spine number, spine density, spine length and dendrite length, and validated their results by comparing them with manual annotations provided by experts. According to these results, the number of detected spines was very close to the manual results; e.g. experts detected 70 spines in a dendrite, which are shown in part (a) of Figure 2.3 whereas NeuronIQ found 4 wrong spines and missed 1. Results of NeuronIQ are shown in part (b) of Figure 2.3. The mean square error (MSE) for the manually and automatically measured spine lengths was 0.0292 μm .

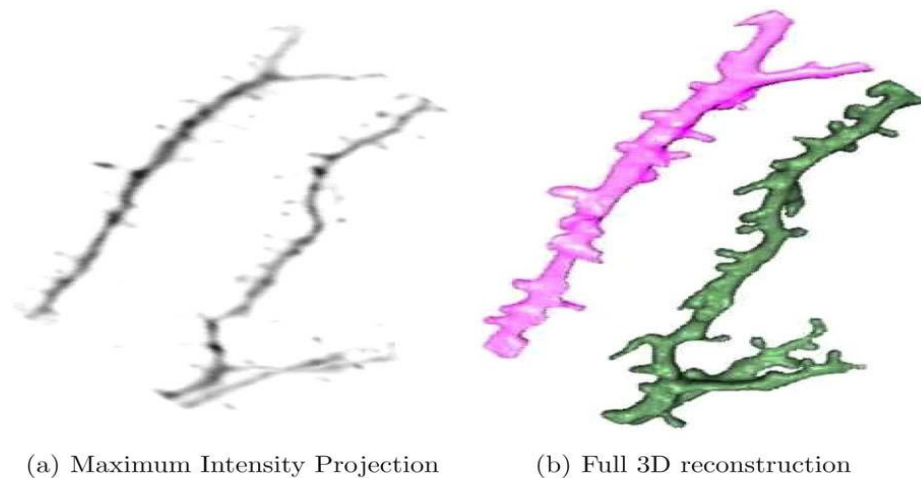
Figure 2.3: Comparison of manual analysis and the results of NeuronIQ.



In some studies researchers focused on 3D reconstruction of dendritic spines for understanding the relation between their morphological and functional properties. For example Janoos et al. (2009) uses images taken by two photon microscopy and

preprocesses them with non-linear filter for noise reduction. Dendrite and spines in these images are segmented using global thresholding and active contour shape models. After image processing, 3D reconstruction is completed using following steps; (1) low-pass filter the surface to remove the high-frequency noise and down-sample to a sufficient resolution, (2) curve-skeletonisation using medial geodesic function, (3) representation of the curve-skeleton with an attributed tree structure that encodes the geometry and topology of the dendrite, (4) detection of dendritic backbone, backbone chain, spine chain and elimination of spurious branches using thresholding with a length-based method. An exemplary MIP image of a neuron and its 3D reconstruction is given in Figure 2.4. In the last part of this study authors compared the spine length, spine volume, and basal, maximum and minimum radius of spine with manual annotations provided by four different users. According to these results this method gives large errors but authors stated this large error to be normal since manual annotations were obtained in 2D.

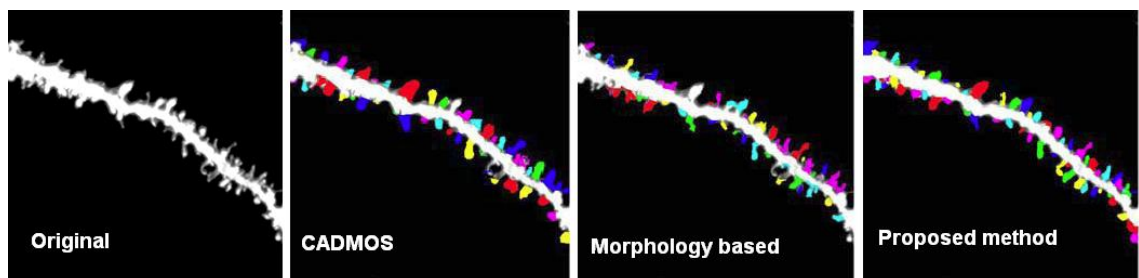
Figure 2.4: 3D reconstruction of a neuron image realized using the method given at Janoos et al. (2009).



Choy et al. (2010) has also mentioned that morphological and statistical properties of dendritic spines are crucial in understanding neurological disorders and also changes in the structure of dendritic spines may have an effect on learning process. In order to investigate the structural changes in dendritic spines, authors proposed model-based curvilinear structure detector with the use of a multi scale spine detection approach. They stated that when working on 2D MIP images some spines are hidden in dendritic area along the optical direction of 3D image stack. Therefore, the number of spines

detected is less than the actual quantity. Therefore the main purpose of their study is to improve the accuracy of spine detection on 2D MIP images. Their method contains two steps; (1) Multi scale spine detection and (2) Slice-based spine detection. In the first step, dendritic backbone was extracted and spines from small scale to large scale were detected using multi scale spine detection method which is an improved version of CADMOS (Curvilinear-based automatic detection and measurement method) given in Zhang's paper. In the second step, spines hidden along the dendrite area is detected using the following steps: (1) Image preprocessing(e.g. median filtering, local adaptive thresholding, and morphological operations), (2) seeded watershed segmentation on each slice to segment individual spines, (3) removing overlapping spines in successive slices, and (4) summing the number of each spine in each slice. Evaluation of this method was obtained using ten fluorescent neuron images taken by a confocal microscope through comparisons with the results of the traditional CADMOS, a morphology based method and manual segmentations. In one image; the traditional CADMOS found 45 spines, the morphology based method found 40 spines and proposed method found 73 spines (slice-based method detects 11 spines; Multi scale spine detection finds 62 spines). Finally, manual segmentation shows 77 spines. In Figure 2.5 visual results of these methods are shown. This method can also be used to obtain spine length and this algorithm obtains an average spine length of 1.187 μm while the manual labeling obtains 1.206 μm .

Figure 2.5: Results given in the study of Choy et al. (2010).



Another dendritic spine analysis method was provided by Son et al. (2010). Images in this study were obtained by confocal microscope and preprocessed with unsharp mask filtering. This filtered image is converted to a binary image using a threshold value. Then dendrite skeleton and spines are obtained applying anisotropic diffusion filtering on this binary image. Dendritic spines are segmented using two consecutive methods;

(1) geodesic active contour method and (2) watershed algorithm. Geodesic active contour method is used for segmentation of spine head, and the initial position of the spine is accepted as the tip of skeleton. But the results of this algorithm can be merged since spines can be too close or intensity difference between them can be small. Therefore, merged spines need to be separated via watershed algorithm, by this way accuracy of segmentation is increased. Segmentation of spines is followed with a classification step. In this part spines are separated into three types; thin, stubby and mushroom. This decision is taken via shape features such as area, location, perimeter, roundness and length of a dendritic spine. Validation of this method is done by comparing the results found with manual results that are provided by three graduate students in Neuroscience. This comparison represented numerically using a sensitivity measure obtained by dividing the number of correctly detected dendritic spines to the sum of both correctly and wrongly detected dendritic spines. According to this measurement, sensitivity of manual detection is 83.1% whereas it is 92.5% for the automated tool.

Recently, Zhang et al. 2010 proposed a new method for detection and segmentation of medium-sized spiny neurons (MSN) using 3D confocal microscopy data. Prior to spine detection, 3D deconvolution is applied as preprocessing, and the foreground-background separation is realized by Otsu thresholding Spine detection consists of two steps; (i) a gradient vector tracking method applied to find candidate feature points close to the central regions of dendrites and spines, and (ii) a Hessian matrix-based eigen-analysis approach applied in order to detect spinal feature points from the whole candidate feature points. Thereafter, Fast Marching algorithm initialized at the detected spinal feature points is employed for spine segmentation. Performance evaluation is accomplished by comparison with manual analysis, where the proposed method correctly detected 1015 spines out of 1123, missed 108, and falsely detected 152. Literature survey showed that dendritic spine analysis consists of four main steps; (1) image preprocessing for noise removal, (2) spine detection, (3) spine segmentation and (4) post processing for analysis of dendritic spines thru volume, length, density, quantity, etc.. In our study we will focus on the segmentation of dendritic spines and in literature there are some approaches for segmentation such as adaptive thresholding (Cheng et al. 2007, Rodriguez et al. 1997, Weaver et al. 2004), global thresholding

(Janoos et al. 2009), watershed segmentation (Choy et al. 2010 and Son et al.2010) and active contour method (Cheng et al. 2007)In this thesis we propose the use of Active Contour with Shape Prior method of Bresson et al. (2006) for better segmentation results that will increase the accuracy of dendritic spine analysis. Moreover, results of this method will be compared with two different approaches: Global (Otsu) Thresholding and an Active Contour based segmentations.

Table 2.1: Summary of literature survey.

Author/year	Image Acquisition	Pre-processing	Spine Detection	Spine Segmentation	Results
Weaver et al. 2004	Confocal laser microscope	Blind deconvolution based commercial tool	Morphology based	Adaptive Thresholding	Detection:330 spines
	1024x1024 pixels	Max. Intensity Projection(MIP)			37 false positives, 55 false negatives
					Segmentation: Not available
Cheng et al. 2007	Two-photon laser microscope	Median Filtering	Thresholding	Adaptive Thresholding	Detection: 229 spines
		Max. Intensity Projection(MIP)	Morphology based	Morphology based	12 false positives, 5 false negatives
					Segmentation: Not available
Bai et al. 2007	Two-photon laser microscope	Blind Deconvolution	Line Detection	Global Thresholding	Detection: 653 spines
	512x512x16 pixels	Median Filtering	Morphology based	Morphology based	90 false positives, 78 false negatives
		Max. Intensity Projection(MIP)			
Zhang et al. 2007	Two-photon laser microscope	Convolve with Gaussian Kernel	Classification based	Global thresholding	Detection: 254 spines
	512x512x11 pixels	Max. Intensity Projection(MIP)		Morphology based	19 false positives, 13 false negatives
					Segmentation: Not available
Rodriguez et al. 2008	Confocal laser microscope	Deconvolve with commercial tool	Clustering based	Local thresholding	Detection: 449 spines, 48 false negative, 91 false positive
	512x512x100 pixels	Max. Intensity Projection(MIP)		Morphology based	Segmentation: Not available
Janoos et al. 2009	Two-photon laser microscope	Deconvolve with commercial tool	Active Contour	Global thresholding	Detection: Sensitivity measure
	512 x512x12 voxels	Max. Intensity Projection(MIP)			Segmentation: Not available
		Gaussian smoothing			

Fan et al. 2009	Two-photon laser microscope	Deconvolve 3D images by Gibson's point spread function	Morphology based	Gaussian derivative kernel with Hessian mat.	Detection: 107 spines
	512x512 pixels	Max. Intensity Projection(MIP)	Medial axis-based	Thresholding	4 false negative, 12 false positive
		Registration using Iterative Closest Point (ICP) algorithm			Segmentation: Not available
Son et al. 2010	Olympus IX-71 inverted microscope	Unsharp mask filtering	Morphology based	Local thresholding	Detection: Sensitivity measure
	A series of 50 2D images	Thresholding Max. Intensity Projection(MIP)	Rule based	Geodesic active contour	Detection: 67 spines, 5 false negative, 2 false positive
		Isotropic diffusion filtering		Watershed algorithm	Segmentation: Not available
Choy et al. 2010	Confocal laser microscope	Median filtering	Curvilinear based	Thresholding	Detection: 149 spines
	Ten fluorescent neuron	Local adaptive thresholding Max. Intensity Projection(MIP)	Gaussian convolution and Hessian matrix	Watershed segmentation	9 false negative, false positive not available
		Morphological operations	Thresholding		Segmentation: Not available
Zhang et al. 2010	Confocal laser microscope	3D deconvolution using Dougherty method	Shape based	Fast Marching Method	Detection: 1123 spines
	512x512x120 pixels	Otsu Thresholding	Eigen-analysis-based		152 false negative, 108 false positive
		Morphological Close Operation			
		Max. Intensity Projection(MIP)			Segmentation: Not available

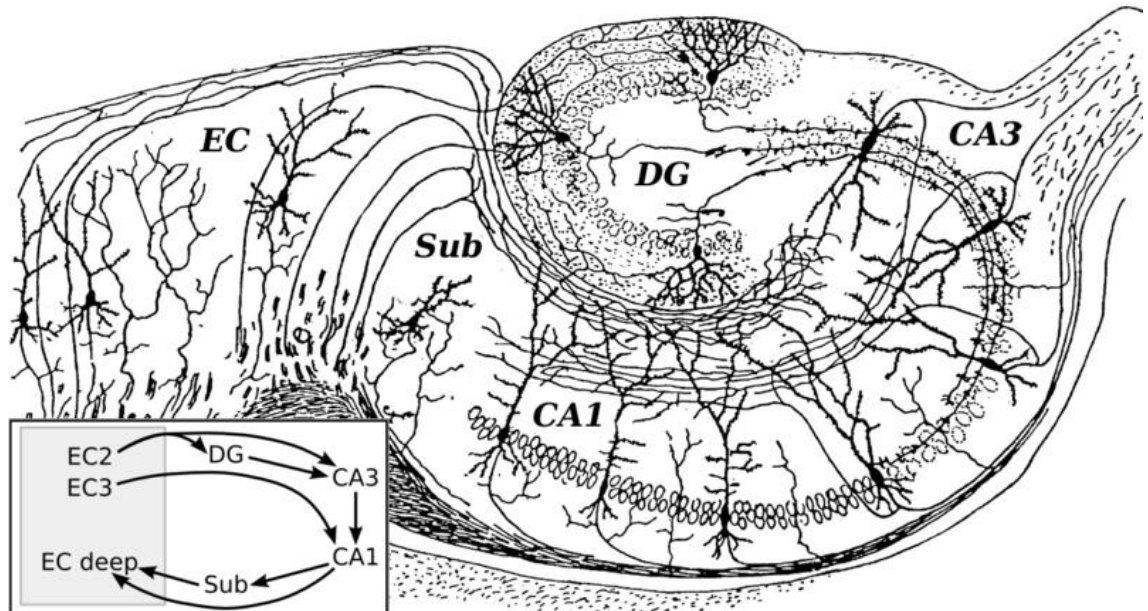
3. METHODS

In this part, following methods used in this study will be explained in the given order; (a) Image acquisition, (b) Region of Interest (ROI) selection, (c) Median Filtering, (d) Global Thresholding based Segmentation, (e) Active Contour based Segmentation and (f) Active Contour with Shape Prior based Segmentation.

3.1 IMAGE ACQUISITION

The images used in this study are acquired by experts from the Neuronal Structure and Function Laboratory in Champalimaud Centre for the Unknown, Lisbon, Portugal using two-photon laser scanning microscope as z-series from secondary dendritic branches of pyramidal neurons in the CA1 region of hippocampus (An example image of hippocampus with the corresponding anatomical annotations is shown in Figure 3.1). Each 1024 X 1024 and 16 bit intensity z-stack contains 25-30 layers and the distance between these layers is 0.3 μm .

Figure 3.1: Image of hippocampus and its regions.



3.2 REGION OF INTEREST (ROI) SELECTION

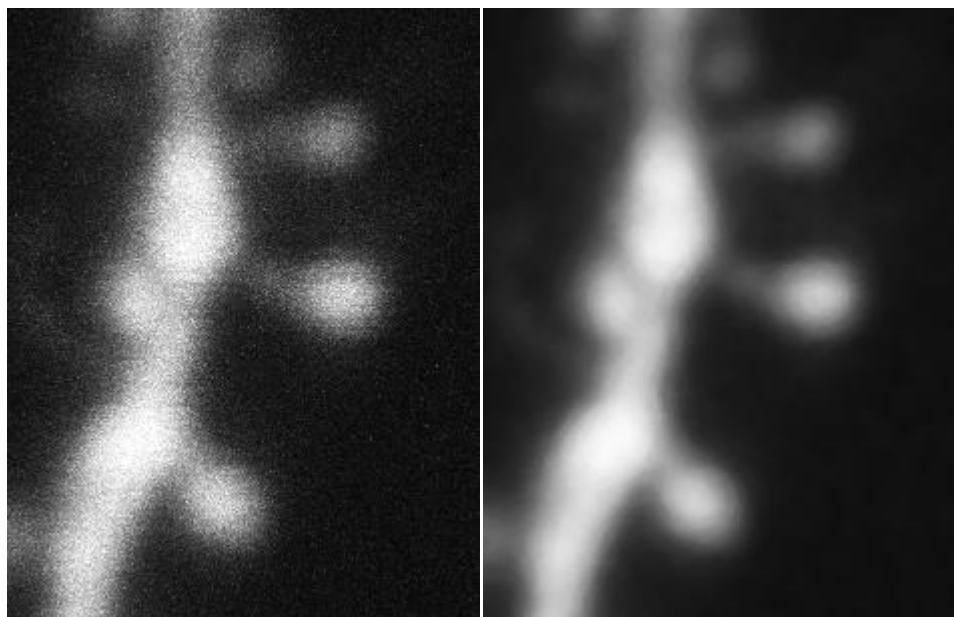
Prior to the segmentation step, a region containing a single spine (both head and neck parts) has to be selected from the dendrite image that is obtained as maximum intensity projection of the image stacks. Depending on the position of the spine (with respect to the dendrite) selected ROI may also contain some parts from the dendrite, which may badly influence the segmentation result.

In order to select a ROI, the user has to place a rectangle around a spine and this rectangle will be ROI. For correct initialization of the active contour based segmentation methods, the spine head has to be at the center of this rectangular ROI.

3.3 DENOISING

Dendrite images taken by two photon microscope contains important amount of noise that can be modeled by the Poisson distribution (Luisier et al. 2009). Therefore, a preprocessing step is needed before applying segmentation algorithms on the images. In this study we used median filtering at the preprocessing step since median filtering is the common method (Choy et al. 2010, Cheng et al. 2007) and etc.) used in the literature for noise reduction. Figure 3.2 shows the result of median filtering applied on the original MIP of a dendrite image from our database.

Figure 3.2: Image on the left is original maximum intensity projection of dendrite image and the image on the right is the median filtered of this image.



3.4 GLOBAL THRESHOLDING BASED SEGMENTATION

As a global thresholding algorithm we chose to use Otsu thresholding in this study. Otsu's method is a technique used for converting grayscale images to binary via an optimum threshold value obtained from the original image (Otsu 1979). This threshold value minimizes the intra-class variance (which is equivalent to maximizing the inter-class variance), and assigns the pixels that has intensity value lower than the threshold as background and other pixels as foreground.

The calculation of the threshold value is very simple and starts with computing histogram and probability of each pixel in a given grayscale image. Then, all pixel values from 1 to the maximum intensity value in the given image are assumed as threshold value iteratively. For each intensity value assumed as threshold, class mean and class probability values are calculated. Furthermore, these values are used to calculate the class variance. After class variance is calculated for each intensity value, the intensity value that gives the maximum inter-class variance defined as threshold value for this method.

3.5 ACTIVE CONTOUR BASED SEGMENTATION

Active contour model, proposed by Chan and Vese (2001), is used for the segmentation of dendritic spines and this model will be explained in this part. Segmentation with an active contour has been realized with curve evolution based on the internal and external energy minimization criteria. In order to calculate the minimization of energy, Mumford-Shah energy function is used in the active contour function of this study.

This method assumes that image is the combination of two regions that has constant intensity values with different values of u_i and u_o . u_i represents inside the region that is aimed to be segmented and whereas u_o represents outside of this region. Basic form of the energy function used in this method given at Equation (3.1).

$$\begin{aligned}
F &= F_1(C) + F_2(C) \\
&= \int_{\text{inside}(C)} |u_0(x,y) - c_1|^2 dx dy \\
&+ \int_{\text{outside}(C)} |u_0(x,y) - c_2|^2 dx dy
\end{aligned} \tag{3.1}$$

In this equation u_0 is the image that will be segmented and C represents the curve that evolves during segmentation, c_1 and c_2 are the constant values that are average intensity value of u_0 both inside and outside of C . As it can be understood from the equation itself, energy will be zero when the evolving curve is at the boundary between two regions that has two distinct intensity values. If the curve is at the outside of the object that will be segmented, $F_1(C)$ becomes larger than zero and $F_2(C)$ is approximately zero. On the other hand, if the curve is at the inside of the object, then $F_2(C)$ becomes larger than zero and $F_1(C)$ is approximately zero. Finally, if the curve is at both inside and outside of the object, then both terms become larger than zero.

Energy function given at Equation (3.1) is extended by adding some regularizing terms like length of the curve C and the area inside the region C and the new energy function showed in Equation (3.2). According to these regularizing terms, curves with smaller area and smoother boundary (i.e. having shorter length) will result in lower energy values.

$$\begin{aligned}
F(c_1, c_2, C) &= \mu . Length(C) + v . Area(C) \\
&+ \lambda_1 . \int_{\text{inside}(C)} |u_0(x,y) - c_1|^2 dx dy \\
&+ \lambda_2 . \int_{\text{outside}(C)} |u_0(x,y) - c_2|^2 dx dy
\end{aligned} \tag{3.2}$$

In this function μ , v , λ_1 and λ_2 are positive, constant and fixed values. In the following parts of this algorithm v is selected as zero whereas λ_1 and λ_2 are selected as equal to the same constant λ . This active contour model is a particular case of the minimal partition problem that can be solved using level set method.

For solving this minimal partition with level set method following expressions are defined.

- a) Variable C used for representation of evolving curve replaced with ϕ , which is a continuous Lipschitz function.
- b) Heaviside function H and one-dimensional Dirac measure δ_0 are defined.

$$H(z) = \begin{cases} 1, & \text{if } z \geq 0 \\ 0, & \text{if } z \leq 0 \end{cases} \quad \delta_0(z) = \frac{d}{dz} H(z) \quad (3.3)$$

- c) Inside of the active contour denoted as ω and outside of the active contour denoted as $\Omega \setminus \omega$.
- d) Terms used in the energy formula has been expressed with formulas shown below in the light of previous definitions.

$$\begin{aligned} \text{Length}\{\phi = 0\} &= \int_{\Omega} |\nabla H(\phi(x, y))| dx dy \\ &= \int_{\Omega} \delta_0(\phi(x, y)) |\nabla \phi(x, y)| dx dy \end{aligned} \quad (3.4)$$

$$\text{Area}\{\phi \geq 0\} = \int_{\Omega} H(\phi(x, y)) dx dy \quad (3.5)$$

$$\int_{\phi > 0} |u_0(x, y) - c_1|^2 dx dy = \int_{\Omega} |u_0(x, y) - c_1|^2 H(\phi(x, y)) dx dy \quad (3.6)$$

$$\begin{aligned} \int_{\phi < 0} |u_0(x, y) - c_2|^2 dx dy &= \int_{\Omega} |u_0(x, y) - c_2|^2 (1 - H(\phi(x, y))) dx dy \end{aligned} \quad (3.7)$$

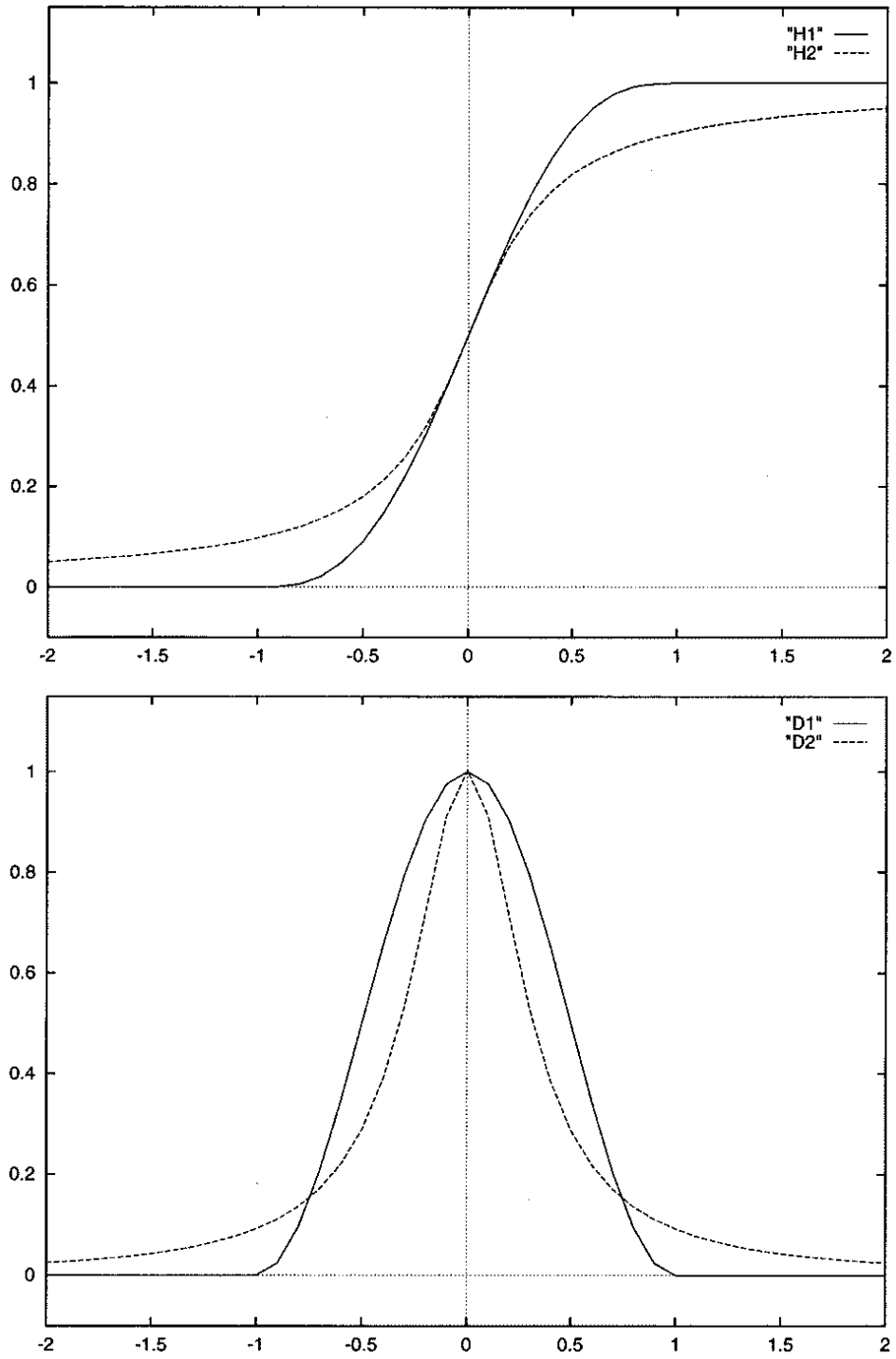
H and δ_0 are discontinuous functions and need to be converted to continuous functions for the subsequent computations. Therefore, they need to be regularized. In Chan and Vese (2001)'s study two different regularizations of H are given and these are shown in Equations (3.8) and (3.9). Regularized version of δ_0 is equal to δ_ϵ which is derivative of H_ϵ .

$$H_{1,\varepsilon}(z) = \begin{cases} 1 & \text{if } z > \varepsilon \\ 0 & \text{if } z < -\varepsilon \\ \frac{1}{2} \left[1 + \frac{z}{\varepsilon} + \frac{1}{\pi} \sin\left(\frac{\pi z}{\varepsilon}\right) \right] & \text{if } |z| \leq \varepsilon \end{cases} \quad (3.8)$$

$$H_{2,\varepsilon}(z) = \frac{1}{2} \left(1 + \frac{2}{\pi} \arctan\left(\frac{z}{\varepsilon}\right) \right) \quad (3.9)$$

In Figure 3.3, graphics for $H_{1,\varepsilon}$, $H_{2,\varepsilon}$, $\delta_{1,\varepsilon}$ and $\delta_{2,\varepsilon}$ are shown. As it can be seen from this figure, $H_{2,\varepsilon}$ and $\delta_{2,\varepsilon}$ are closer to the ideal case. Therefore, they are chosen for the implementation of the algorithm.

Figure 3.3: Graphics of regularized H_ε and δ_ε .



By using the expressions given before and replacing H and δ_0 with their slightly regularized versions which are H_ϵ and δ_ϵ , energy formula can be revised as,

$$\begin{aligned}
F_\epsilon(c_1, c_2, \phi) &= \mu \int_{\Omega} \delta_\epsilon(\phi(x, y)) |\nabla \phi(x, y)| dx dy \\
&+ \nu \int_{\Omega} H_\epsilon(\phi(x, y)) dx dy \\
&+ \lambda \int_{\Omega} |u_0(x, y) - c_1|^2 H_\epsilon(\phi(x, y)) dx dy \\
&+ \lambda \int_{\Omega} |u_0(x, y) - c_2|^2 (1 - H_\epsilon(\phi(x, y))) dx dy
\end{aligned} \tag{3.10}$$

Euler-Lagrange equation for ϕ is obtained by keeping c_1 and c_2 fixed, and minimizing F_ϵ with respect to ϕ in the energy function (Equation 3.11). In this equation direction is parameterized with an artificial time t in equation $\phi(t, x, y)$ which is used as $\phi(0, x, y)$. In this function $div\left(\frac{\nabla \phi}{|\nabla \phi|}\right)$ is equal to the curvature of the active contour function.

$$\begin{aligned}
\frac{\partial \phi}{\partial t} &= \delta_\epsilon(\phi) \left[\mu \operatorname{div} \left(\frac{\nabla \phi}{|\nabla \phi|} \right) - \nu - \lambda(u_0 - c_1)^2 + \lambda(u_0 - c_2)^2 \right] \\
&= 0 \text{ in } (0, \infty) \times \Omega,
\end{aligned}$$

$$\phi(0, x, y) = \phi_0(x, y) \text{ in } \Omega,$$

$$\frac{\delta_\epsilon(\phi)}{|\nabla \phi|} \frac{\partial \phi}{\partial \vec{n}} = 0 \text{ in } \partial \Omega,$$

$$\text{where } \vec{n} \text{ denotes the exterior normal to boundary} \tag{3.11}$$

Main steps of this algorithm are listed below:

- i. Initialize ϕ^0 with initial curve where ϕ denotes a Lipschitz function that represents the evolving curve C .
- ii. Compute $c_1(\phi^n)$ and $c_2(\phi^n)$ where c_1 represents the average intensity values inside and on the boundary of C , and c_2 represents the average intensity values outside C .
- iii. Solve Equation (3.11) in order to calculate the evolving curve ϕ^{n+1} from ϕ^n .

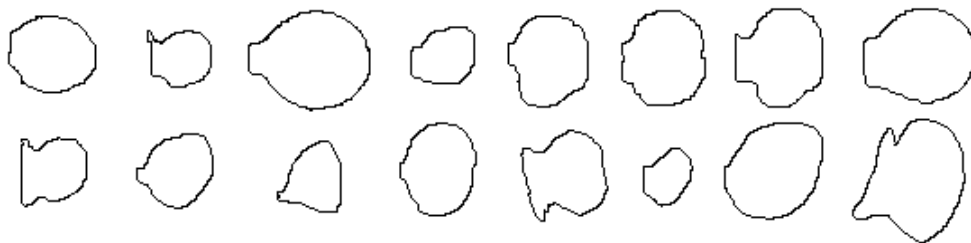
- iv. ϕ can be (optionally) initialized again locally with the Signed Distance Function(SDF) to the curve.
- v. Mumford-Shah energy function is checked. If the result is stationary then the algorithm will stop. Otherwise, it will continue with a new iteration, represented by $n+1$.

3.6 ACTIVE CONTOUR WITH SHAPE PRIOR BASED SEGMENTATION

Active Contour with Shape Prior method proposed by Bresson et al. (2006) is used in this thesis and will be explained in this part. According to this method dendritic spines are segmented using three techniques; active contour method, energy minimization function and shape knowledge. This algorithm is similar to the active contour method explained in part (3.5). This algorithm also stops according to the minimization of energy function but in this algorithm energy function is not calculated using only the Mumford-Shah function. It is calculated using three different terms; boundary term, shape term and region term. Boundary term is resulted from image gradients, shape term is obtained from the shape knowledge and region term is calculated using the intensity values in the segmented region via Mumford-Shah function. This minimum energy function is solved using the level set method.

In this algorithm shape variation is needed in order to calculate the total energy function. For obtaining this shape variation, in this study a training set containing 16 spine images is created and used (Figure 3.3). Note that this training set is different from the test set used to evaluate the performances of the segmentation algorithms.

Figure 3.4: Training set.



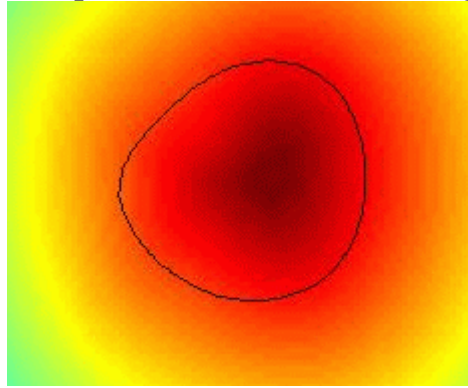
Principal Component Analysis (PCA) is applied on this training set. By this way common properties of the spine images in the training set have been obtained and unnecessary information of the images are removed. As a result a mean shape ($\bar{\phi}$) - used

as the initial curve C , p principal components \mathbf{x}_{pca} - sorted in a matrix W_p - and their corresponding eigen coefficients vector (\mathbf{x}_{pca}) have been created. By using these values, a shape function, given in Equation (3.12), has been defined.

$$\hat{\phi} = \bar{\phi} + W_p \mathbf{x}_{pca} \quad (3.12)$$

PCA is not applied directly to the images in the training set, but to the Signed Distance Functions (SDF) of these images. By this way representation of images in the training set is realized implicitly and with less parameter. This brings in two advantages (i) SDF results are more tolerant to misalignment, (ii) shape registration process becomes more robust, more accurate and faster.

Figure 3.5: Mean shape obtained from the training set (Figure 3.4).



In Figure 3.5, black curve is the mean shape that is constructed from training set using PCA.

Energy function of this method is calculated using Equation (3.13).

$$F = \beta_s \times F_{\text{shape}}(C, \mathbf{x}_{pca}, \mathbf{x}_T) + \beta_b \times F_{\text{boundary}}(C) + \beta_r \times F_{\text{region}}(\mathbf{x}_{pca}, \mathbf{x}_T, u_{\text{in}}, u_{\text{out}}) \quad (3.13)$$

In this formula F_{shape} , F_{boundary} and F_{region} represents the energy values resulted from shape, boundary and region terms. β_s , β_b and β_r are constant values that define the weights of each energy terms.

F_{shape} is calculated based on the active contour C , $\hat{\phi}$ is the shape function of the object of interest given by the PCA, \mathbf{x}_{pca} is the Eigen coefficients vector obtained after applying

PCA on the SDF's of images in the training set, and \mathbf{x}_T is the vector of geometric transformation, which is defined with a function, $h_{\mathbf{x}_T}$. Geometric transformations vector can be a vector of 2-D rigid or affine transformations. Rigid transformation contains the following terms; a scale parameter(s), an angle of rotation(θ) and a vector of translations(T). On the other hand, affine transformation further includes a shearing parameter(s_h). In Equations (3.14) and (3.15), definitions of geometric transformation are given for both rigid ($h_{\mathbf{x}_T^r}$) and affine ($h_{\mathbf{x}_T^a}$) transformations.

$$h_{\mathbf{x}_T^r} = x \rightarrow h_{(s,\theta,T)}(x) = s R_\theta x + T \quad (3.14)$$

$$h_{\mathbf{x}_T^a} = x \rightarrow h_{(s_x,s_y,\theta,s_h,T)}(x) = R_{sc} R_\theta R_{sh} x + T \quad (3.15)$$

Matrices used in the previous equations for corresponding geometric transformation parameters are shown in Equation (3.16).

$$R_{sc} = \begin{pmatrix} s_x & 0 \\ 0 & s_y \end{pmatrix}, R_\theta = \begin{pmatrix} \cos \theta & \sin \theta \\ -\sin \theta & \cos \theta \end{pmatrix}, R_{sh} = \begin{pmatrix} 1 & s_h \\ 0 & 1 \end{pmatrix}, T = \begin{pmatrix} T_x \\ T_y \end{pmatrix} \quad (3.16)$$

Equation for the calculation of F_{shape} is shown below with Equation (3.17), which calculates the similarity between the active contour and the shape prior that is to be segmented. This function measures the similarity by calculating the sum-of-square-differences between the shape model and the active contour.

$$F_{\text{shape}} = \int_0^1 \widehat{\phi}^2(\mathbf{x}_{\text{pca}}, h_{\mathbf{x}_T}(C(q))) |C'(q)| dq \quad (3.17)$$

This equation can be minimized by applying the calculus of variations and gradient descent methods on the three terms of F_{shape} . Each of these terms can be analyzed by fixing the other two.

Minimization of F_{shape} according to active contour C by fixing \mathbf{x}_{pca} and \mathbf{x}_T can be done by solving Equation (3.18). In this equation there are two terms; (a) the mean curvature term which is weighted by the square of shape function $\widehat{\phi}$ and (b) the factor that pushes C towards the zero level set of $\widehat{\phi}$. This function deforms the shape of active contour to any shape of the PCA model. Change in the shape of active contour has two benefits; independency from parametric contour representation as a result of intrinsic level set

representation and being more accurate than the change occurred in parametric contours since level set functions has higher degree of deformation.

$$\partial_t C(t, q) = (\widehat{\phi} \kappa - \langle \nabla \widehat{\phi}^2, \mathcal{N} \rangle) \mathcal{N}, \text{ where } (t, q) \in]0, \infty[\times]0, 1],$$

$$C(0, q) = C_0(q), \text{ where } q \in [0, 1] \quad (3.18)$$

Equation (3.19) can be used to show the minimization process of F_{shape} according to the \mathbf{x}_{pca} , the Eigen coefficients vector by fixing C and \mathbf{x}_T .

$$d_t x_{\text{pca}}(t) = -2 \int_0^1 \widehat{\phi} (\nabla_{\mathbf{x}_{\text{pca}}} \widehat{\phi}) |C'| dq,$$

$$\text{where } (t, \mathbf{x}_{\text{pca}}) \in]0, \infty[\times \Omega_{\text{pca}},$$

$$x_{\text{pca}}(t = 0) = x_{\text{pca}_0}, \text{ where } \mathbf{x}_{\text{pca}} \in \Omega_{\text{pca}}$$

$$\nabla_{\mathbf{x}_{\text{pca}}} \widehat{\phi} = (e_{\text{pca}}^1 \dots \dots e_{\text{pca}}^p) \quad (3.19)$$

where e_{pca}^i represents the i th eigenvector obtained from PCA and Ω_{pca} is the PCA variables space. The shape function $\widehat{\phi}$ changes with this equation in order to match its zero level set with the active contour.

F_{shape} can also be minimized according to the geometric transformations vector, \mathbf{x}_T by fixing \mathbf{x}_{pca} and C . This minimization term can be expressed with Equation (3.20).

$$d_t x_T(t) = -2 \int_0^1 \widehat{\phi} \langle \nabla \widehat{\phi}, \nabla_{\mathbf{x}_T} h_{\mathbf{x}_T}(C) \rangle |C'| dp,$$

$$\text{where } (t, \mathbf{x}_T) \in]0, \infty[\times \Omega_T,$$

$$x_T(t = 0) = x_{T_0}, \text{ where } \mathbf{x}_T \in \Omega_T \quad (3.20)$$

The gradient term $\nabla_{\mathbf{x}_T} h_{\mathbf{x}_T}$ given in Equation (3.20) corresponds to the partial derivatives of the geometric transformation function $h_{\mathbf{x}_T}$ with respect to the parameters of the geometric transformation vector \mathbf{x}_T . Definitions of $\nabla_{\mathbf{x}_T} h_{\mathbf{x}_T}$ are given in Equations (3.21) and (3.22) for 2-D rigid and affine transformations, respectively.

$$\nabla_{x_T^r} h_{x_T}(x) = \begin{pmatrix} \frac{\partial h_{x_T^r}(x)}{\partial s} = R_\theta x \\ \frac{\partial h_{x_T^r}(x)}{\partial \theta} = s(\partial_\theta R_\theta)x \\ \frac{\partial h_{x_T^r}(x)}{\partial T} = 1 \end{pmatrix} \quad (3.21)$$

$$\nabla_{x_T^a} h_{x_T}(x) = \begin{pmatrix} \frac{\partial h_{x_T^a}(x)}{\partial s_x} = (\partial_{s_x} R_{sc}) R_\theta R_{sh} x \\ \frac{\partial h_{x_T^a}(x)}{\partial s_y} = (\partial_{s_y} R_{sc}) R_\theta R_{sh} x \\ \frac{\partial h_{x_T^a}(x)}{\partial \theta} = R_{sc} (\partial_\theta R_\theta) R_{sh} x \\ \frac{\partial h_{x_T^a}(x)}{\partial sh} = R_{sc} R_\theta (\partial_{sh} R_{sh}) x \\ \frac{\partial h_{x_T^a}(x)}{\partial T} = 1 \end{pmatrix} \quad (3.22)$$

In order to solve these equations, they need to be defined as variational level set formulations. Level set formulation defined for the energy function of shape; F_{shape} from Equation (3.17) is given in Equation (3.23).

$$F_{shape} = \int_{\Omega} \widehat{\varphi}^2(x_{pca}, h_{x_T}(x)) |\nabla \varphi| \delta(\varphi) d\Omega \quad (3.23)$$

In this equation φ is a level set function embedding the active contour C , $\delta(\cdot)$ is the Dirac function and $\delta(\varphi)$ is the contour measure on $\{\varphi=0\}$.

Equations (3.18), (3.19) and (3.20) are reformulated according to the level set model in the following equations. These new equations are used to control the shape of active contour that has to be consistent with the shape prior.

$$\partial_t \varphi(t, x) = \left(\widehat{\varphi}^2 \kappa - \langle \nabla \widehat{\varphi}^2, \frac{\nabla \varphi}{|\nabla \varphi|} \rangle \right) \delta(\varphi), \text{ where } (t, x) \in]0, \infty[\times \Omega,$$

$$\varphi(0, x) = \varphi_0(x), \text{ where } x \in \Omega, \quad (3.24)$$

$$\frac{\delta(\varphi)}{|\nabla\varphi|} \partial_{\mathcal{N}}\varphi = 0 \text{ on } \partial\Omega$$

$$d_t x_{pca}(t) = -2 \int_{\Omega} \widehat{\phi} \nabla_{x_{pca}} \widehat{\phi} |\nabla\varphi| \delta(\varphi) d\Omega ,$$

$$\text{where } (t, x_{pca}) \in]0, \infty[\times \Omega_{pca},$$

$$x_{pca}(t = 0) = x_{pca_0} \text{ where } x_{pca} \in \Omega_{pca} \quad (3.25)$$

$$d_t x_T(t) = -2 \int_0^1 \widehat{\phi} \langle \nabla\widehat{\phi}, \nabla_{x_T} h_{x_T} \rangle |\nabla\varphi| \delta(\varphi) d\Omega ,$$

$$\text{where } (t, x_T) \in]0, \infty[\times \Omega_T,$$

$$x_T(t = 0) = x_{T_0}, \text{ where } x_T \in \Omega_T \quad (3.26)$$

F_{region} term is calculated using Mumford-Shah energy function in order to obtain a smooth region as a result of segmentation. Mumford-Shah energy function is applied on the shape prior instead of active contour. Because when it is applied to active contour, it will end up with a segmentation result that is a homogenous region without any shape. Therefore, Mumford-Shah energy function has to be applied to region that is restricted with shape information. Equation used for the calculation of F_{region} is given in Equation (3.27).

$$\begin{aligned} F_{\text{region}} = & \int_{\Omega_{in}(x_{pca}, x_T)} (|I - u_{in}|^2 + \mu |\nabla u_{in}|^2 d\Omega) \\ & + \int_{\Omega_{out}(x_{pca}, x_T)} (|I - u_{out}|^2 + \mu |\nabla u_{out}|^2 d\Omega) \end{aligned} \quad (3.27)$$

In this equation Ω_{in} and Ω_{out} respectively represents the region inside and outside of the curve C. u_{in} is the smooth approximation of intensity inside the curve C whereas u_{out} is the smooth approximation of intensity outside the curve C. This equation is rewritten using the shape function $\widehat{\phi}$ and Heaviside function H in Equation (3.28).

$$\begin{aligned}
F_{region}(x_{pca}, x_T, u_{in}, u_{out}) &= \int_{\Omega} (|I - u_{in}|^2 + \mu |\nabla u_{in}|^2) H(\widehat{\Phi}(x_{pca}, x_T)) d\Omega \\
&+ \int_{\Omega} (|I - u_{out}|^2 + \mu |\nabla u_{out}|^2) H(-\widehat{\Phi}(x_{pca}, x_T)) d\Omega
\end{aligned} \tag{3.28}$$

Energy function based on the region term can be minimized using the gradient descent method for x_{pca} and x_T , and solving the Euler- Lagrange equations for u_{in} and u_{out} . Results obtained by this way can be seen in the following equations.

$$\begin{aligned}
d_t x_{pca}(t) &= \int_{\Omega} ((|I - u_{in}|^2 + \mu |\nabla u_{in}|^2) \\
&- (|I - u_{out}|^2 + \mu |\nabla u_{out}|^2)) \frac{\partial \widehat{\Phi}}{\partial x_{pca}} \delta(\widehat{\Phi}) d\Omega, \\
&= \int_{\Omega} ((|I - u_{in}|^2 + \mu |\nabla u_{in}|^2) \\
&- (|I - u_{out}|^2 + \mu |\nabla u_{out}|^2)) \nabla_{x_{pca}} \widehat{\Phi} \delta(\widehat{\Phi}) d\Omega, \\
&\text{where } (t, x_{pca}) \in]0, \infty[\times \Omega_{pca}, \\
x_{pca}(t = 0) &= x_{pca_0} \text{ where } x_{pca} \in \Omega_{pca}
\end{aligned} \tag{3.29}$$

$$\begin{aligned}
d_t x_T(t) &= \int_{\Omega} ((|I - u_{in}|^2 + \mu |\nabla u_{in}|^2) \\
&- (|I - u_{out}|^2 + \mu |\nabla u_{out}|^2)) \frac{\partial \widehat{\Phi}}{\partial x_T} \delta(\widehat{\Phi}) d\Omega, \\
&= \int_{\Omega} ((|I - u_{in}|^2 + \mu |\nabla u_{in}|^2) \\
&- (|I - u_{out}|^2 + \mu |\nabla u_{out}|^2)) \langle \nabla \widehat{\Phi}, \nabla_{x_T} h_{x_T} \rangle \delta(\widehat{\Phi}) d\Omega, \\
&\text{where } (t, x_T) \in]0, \infty[\times \Omega_T, \\
x_T(t = 0) &= x_{T_0} \text{ where } x_T \in \Omega_T
\end{aligned} \tag{3.30}$$

$$\partial_T u_{in}(t, x) = u_{in} - I - \mu \Delta u_{in} \text{ where } (t, x) \in]0, \infty[\times \{\widehat{\phi} > 0\},$$

$$u_{in}(0, x) = I \text{ where } x \in \{\widehat{\phi} > 0\}$$

$$\partial_T u_{out}(t, x) = u_{out} - I - \mu \Delta u_{out} \text{ where } (t, x) \in]0, \infty[\times \{\widehat{\phi} < 0\},$$

$$u_{out}(0, x) = I \text{ where } x \in \{\widehat{\phi} < 0\} \quad (3.31)$$

F_{boundary} term is calculated using following Equation (3.32) that is obtained from the local image information resulted from the image gradients and edge detection.

$$F_{\text{boundary}} = \oint_0^1 g(|\nabla I(C(q))|) |C'(q)| dq \quad (3.32)$$

Energy terms based on shape, region and boundary terms are combined and expressed according to the level set method in Equation (3.33).

$$\begin{aligned} F = & \int_{\Omega} (\beta_s \widehat{\phi}^2 (x_{pca}, h_{x_T}(x)) + \beta_b g(|\nabla I(x)|) |\nabla \phi| \delta(\phi)) d\Omega \\ & + \beta_r \int_{\Omega} (((|I - u_{in}|^2 + \mu |\nabla u_{in}|^2) H(\widehat{\phi}(x_{pca}, x_T)) \\ & + ((|I - u_{out}|^2 + \mu |\nabla u_{out}|^2) H(-\widehat{\phi}))) d\Omega \end{aligned} \quad (3.33)$$

Minimization equations shown in Equations (3.34), (3.35), (3.36) and (3.37) are obtained using gradient descent method and solutions of Euler- Lagrange equations on energy function F.

$$\partial_t \phi(t, x) = \left(f_k - \langle \nabla f, \frac{\nabla \phi}{|\nabla \phi|} \rangle \right) \delta(\phi), \text{ where } (t, x) \in]0, \infty[\times \Omega,$$

$$\phi(0, x) = \phi_0(x), \text{ where } x \in \Omega,$$

$$\frac{\delta(\phi)}{|\nabla \phi|} \partial_N \phi = 0 \text{ on } \partial \Omega \quad (3.34)$$

$$\begin{aligned}
d_t x_{pca}(t) = & - \int_{\Omega} \left(\nabla_{x_{pca}} \widehat{\varphi} \left(2\beta_s \widehat{\varphi} |\nabla \varphi| \delta(\varphi) \right. \right. \\
& + \beta_r \left((|I - u_{in}|^2 + \mu |\nabla u_{in}|^2) - (|I - u_{out}|^2 \right. \\
& \left. \left. + \mu |\nabla u_{out}|^2) \right) \delta(\widehat{\varphi}) \right) d\Omega, \\
& \text{where where } (t, x_{pca}) \in]0, \infty[\times \Omega_{pca}, \\
x_{pca}(t = 0) = & x_{pca_0} \text{ where } x_{pca} \in \Omega_{pca}
\end{aligned} \tag{3.35}$$

$$\begin{aligned}
d_t x_T(t) = & - \int_{\Omega} \left(\langle \nabla \widehat{\varphi}, \nabla_{x_T} h_{x_T} \rangle \left(2\beta_s \widehat{\varphi} |\nabla \varphi| \delta(\varphi) \right. \right. \\
& + \beta_r \left((|I - u_{in}|^2 + \mu |\nabla u_{in}|^2) - (|I - u_{out}|^2 \right. \\
& \left. \left. + \mu |\nabla u_{out}|^2) \right) \delta(\widehat{\varphi}) \right) d\Omega, \\
& \text{where where } (t, x_T) \in]0, \infty[\times \Omega_T, \\
x_T(t = 0) = & x_{T_0} \text{ where } x_T \in \Omega_T
\end{aligned} \tag{3.36}$$

$$\begin{aligned}
\partial_T u_{in}(t, x) = & u_{in} - I - \mu \Delta u_{in} \text{ where } (t, x) \in]0, \infty[\times \{\widehat{\varphi} > 0\}, \\
u_{in}(0, x) = & I \text{ where } x \in \{\widehat{\varphi} > 0\} \\
\partial_T u_{out}(t, x) = & u_{out} - I - \mu \Delta u_{out} \text{ where } (t, x) \in]0, \infty[\times \{\widehat{\varphi} < 0\}, \\
u_{out}(0, x) = & I \text{ where } x \in \{\widehat{\varphi} < 0\}
\end{aligned} \tag{3.37}$$

In order to solve these energy minimization Equations (3.34) to (3.37), steps listed below are followed in an iterative manner (Bresson et al. 2006).

- i. Computation of shape function $\widehat{\varphi}(x_{pca}, x_T)$,
- ii. Applying geometric transformation using B-splines interpolation method (Unser 1999),
- iii. Calculation of the gradient vectors using the central difference scheme,

- iv. Discretization of terms $|\nabla\varphi|$ and $\langle \nabla f, \frac{\nabla\varphi}{|\nabla\varphi|} \rangle$ using the Osher-Sethian numerical scheme (Osher and Sethian 1988),
- v. Curvature computation with the central difference scheme.
- vi. Computation of the smooth approximations of intensity values inside and outside the curve C using the equation (3.37),
- vii. Re-distance the level set function with the Fast Marching Method using the method proposed in Adalsteinsson and Sethian (1995).

After some iterations energy function F starts to give stationary results (convergence is achieved). In this study the active contour obtained at 150th iteration (decided according to experimental results) or there is no change for 30 iterations is defined as the resulting segmentation, and this method is implemented using MATLAB.

4. RESULTS

In order to validate the results of dendritic spine segmentation methods, we have used 12 different dendritic spine images (test set) acquired and manually segmented as ground truth by the experts from Neuronal Structure and Function Laboratory in Champalimaud Centre for the Unknown, Lisbon, Portugal. The training and test sets do not overlap.

Evaluation of segmentation accuracy is realized by the Dice Coefficient, defined as the volume of overlap between the manual and automated segmentations normalized by their mean volume, where higher scores indicate better agreement between the two segmentations. Equation (4.1) is used for the calculation of Dice score. In this equation x represents the manual segmentation of dendritic spine, whereas y represents the result of segmentation result obtained using an automated segmentation method.

$$D(x, y) = \frac{2 |x \cap y|}{|x| + |y|} \quad (4.1)$$

In the following sections we first explain the selection of median filter size based on experimental results. Then, the results of each algorithm will be presented separately using both Dice scores and visual results that contain four different images: First will show the whole dendrite image and the ROI we selected, second will display the zoomed image of the ROI, third will present the manual segmentation result overlaid on the original zoomed image and colored with blue, and in the fourth segmentation result obtained with segmentation methods will be presented as overlaid on the original zoomed image and colored with red.

4.1 SELECTION OF MEDIAN FILTER SIZE

The images of dendritic spines taken by two photon microscope are very noisy, and therefore they need to be preprocessed beforehand. In this thesis we preferred median filtering due to its low computational complexity, ease of use, and adequate accuracy. For this part we tried different filter sizes ranging from 3x3 to 19x19. In Table 4.1, Dice scores obtained in the early stages of our study.

Table 4.1: Dice scores obtained in the early stages of the study for Active Contour with Shape Prior method.

Filter Size	3x3	5x5	7x7	9x9	11x11	13x13	15x15	17x17	19x19
Mean Value	0,75	0,81	0,77	0,72	0,78	0,77	0,75	0,77	0,73
Standard Deviation	0,16	0,06	0,08	0,10	0,08	0,10	0,12	0,13	0,16

According to these results, filter sizes of 3x3, 13x13, 15x15, 17x17 and 19x19 were eliminated and not used in the following stages of the thesis. Whereas, segmentation results were obtained using median filter with 5x5, 7x7, 9x9 and 11x11 sizes in further stages of the study. In Table 4.2, final segmentation results using Active Contour with Shape Prior method are given for each filter.

Table 4.2: Dice scores obtained in the final stage of the study for Active Contour with Shape Prior method.

Filter Size	5x5	7x7	9x9	11x11
Mean Value	0,80	0,78	0,83	0,83
Standard Deviation	0,09	0,09	0,06	0,06

As a result, 11x11 filter size is selected as the optimum median filter size since it has high Dice score and low standard deviation and in the following sections results of dendritic spine segmentation are given using this filter size.

4.2 RESULTS OF GLOBAL THRESHOLDING BASED SEGMENTATION

The mean and standard deviation for the Dice scores of Otsu thresholding are measured as 0.68 and 0.198, respectively. Figures (4.1) and (4.2) show exemplary segmentation results with Otsu thresholding.

Figure 4.1: Exemplary segmentation with Otsu Thresholding of Spine 1 (Dice score=0.54). Blue corresponds manual segmentation and red represents automated segmentation.

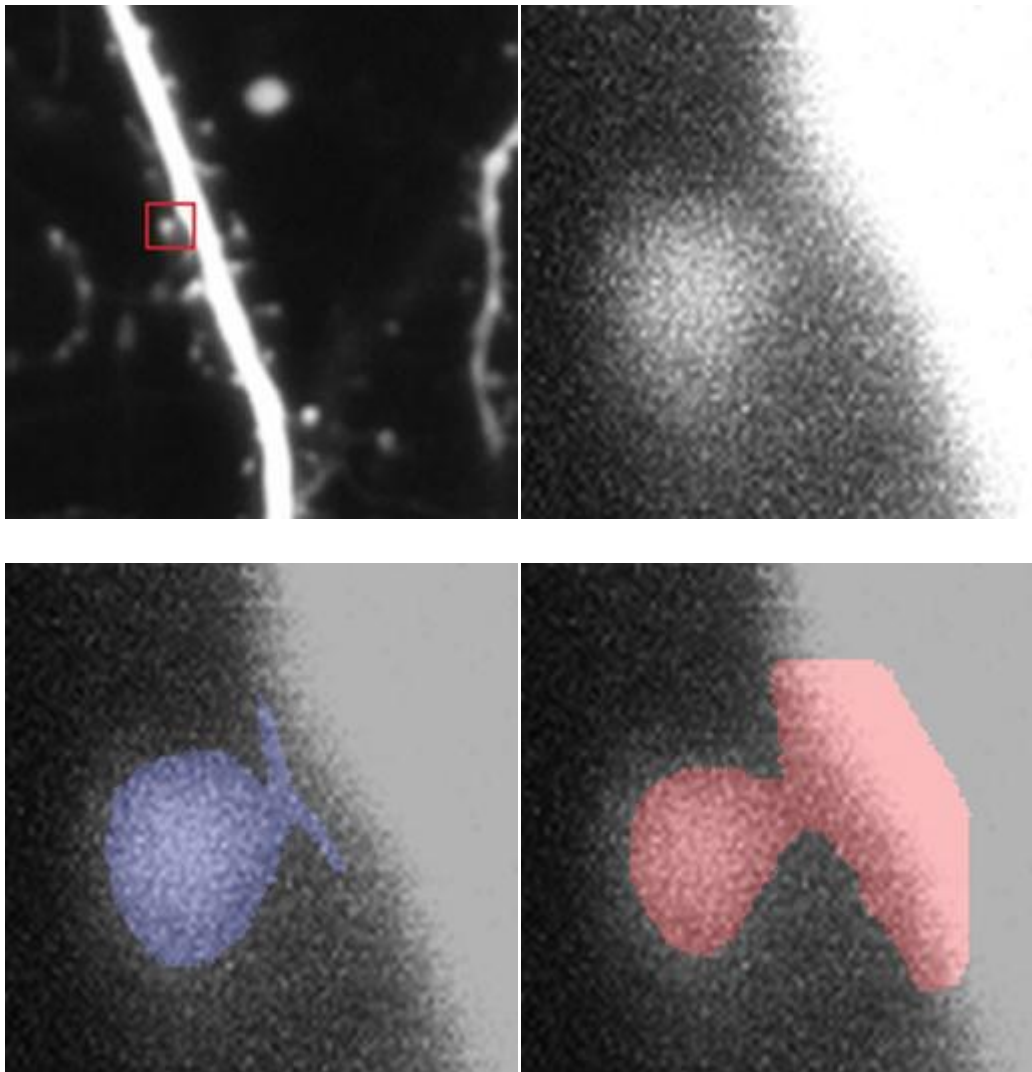
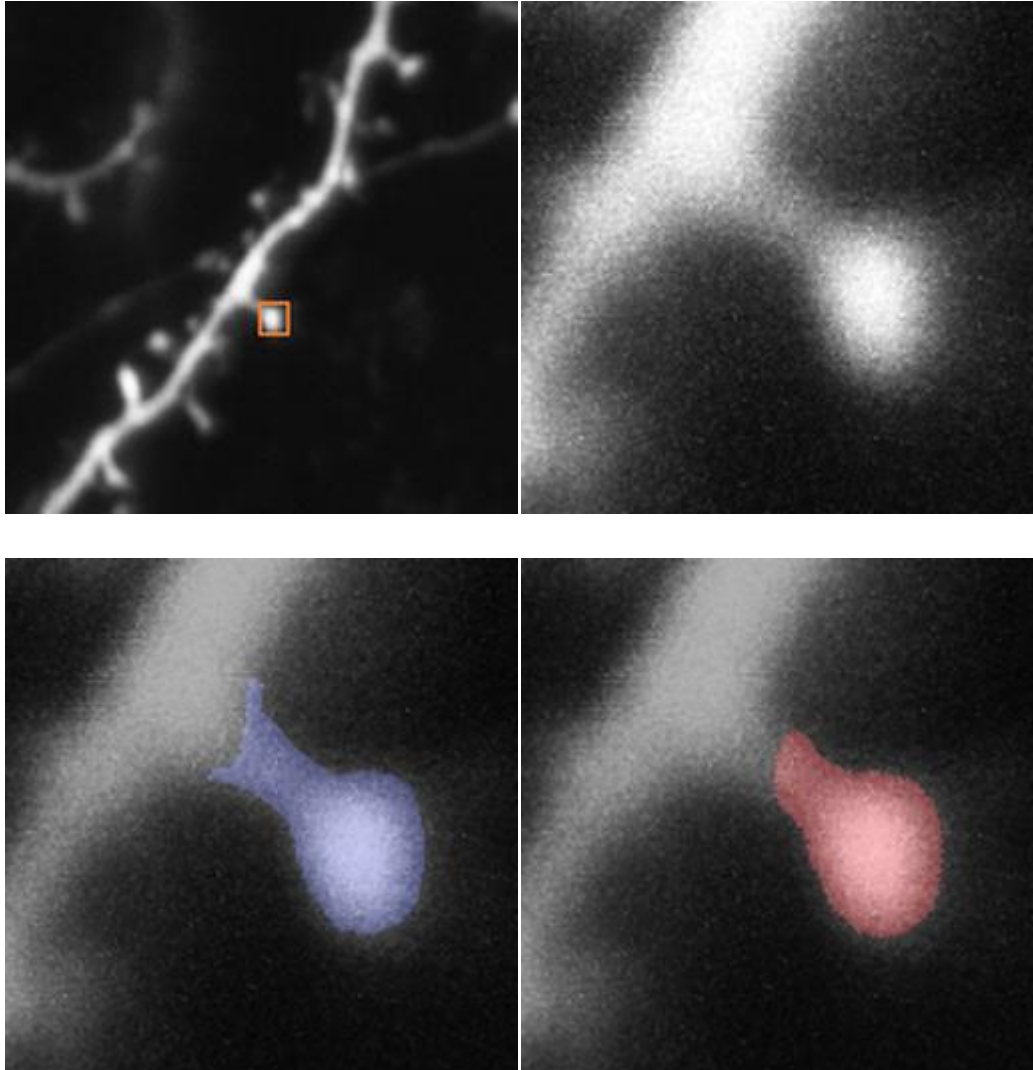


Figure 4.2: Exemplary segmentation with Otsu Thresholding of Spine 8 (Dice score=0.91). Blue corresponds manual segmentation and red represents automated segmentation.



As it can be seen from the Figures 4.1 and 4.2, the success of global thresholding based segmentation depends on the selection of ROI. If ROI contains only the spine head and neck, better segmentation can be achieved. On the other hand, if it contains some parts from dendrite as well, segmentation becomes worse since this method cannot separate the dendrite from the spine.

4.3 RESULTS OF ACTIVE CONTOUR BASED SEGMENTATION

Active contour method needs an initial curve as a starting point for curve evolution. In the ROI selection step we select the ROI such that the spine head remains in the middle of the ROI, and we place the initial curve at the center of the ROI.

Active contour based spine segmentation generally results in better segmentations in comparison to the use of Otsu thresholding. The mean and standard deviation for the Dice scores of active contour based segmentation are measured as 0.769 and 0.110, respectively. Example segmentation results are shown in Figures (4.3) and (4.4).

Figure 4.3: Exemplary segmentation with Active Contour of Spine 1 (Dice score=0.8). Blue corresponds manual segmentation and red represents automated segmentation.

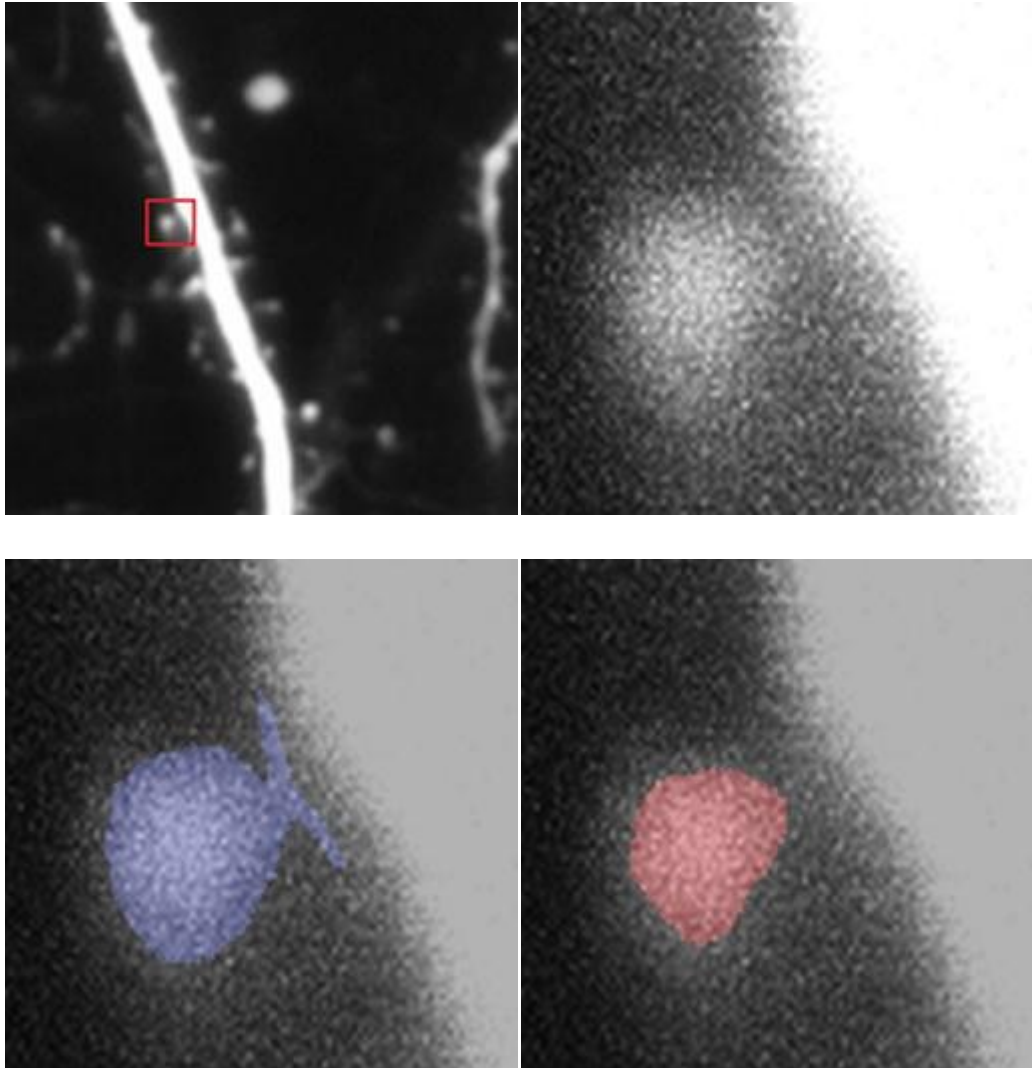
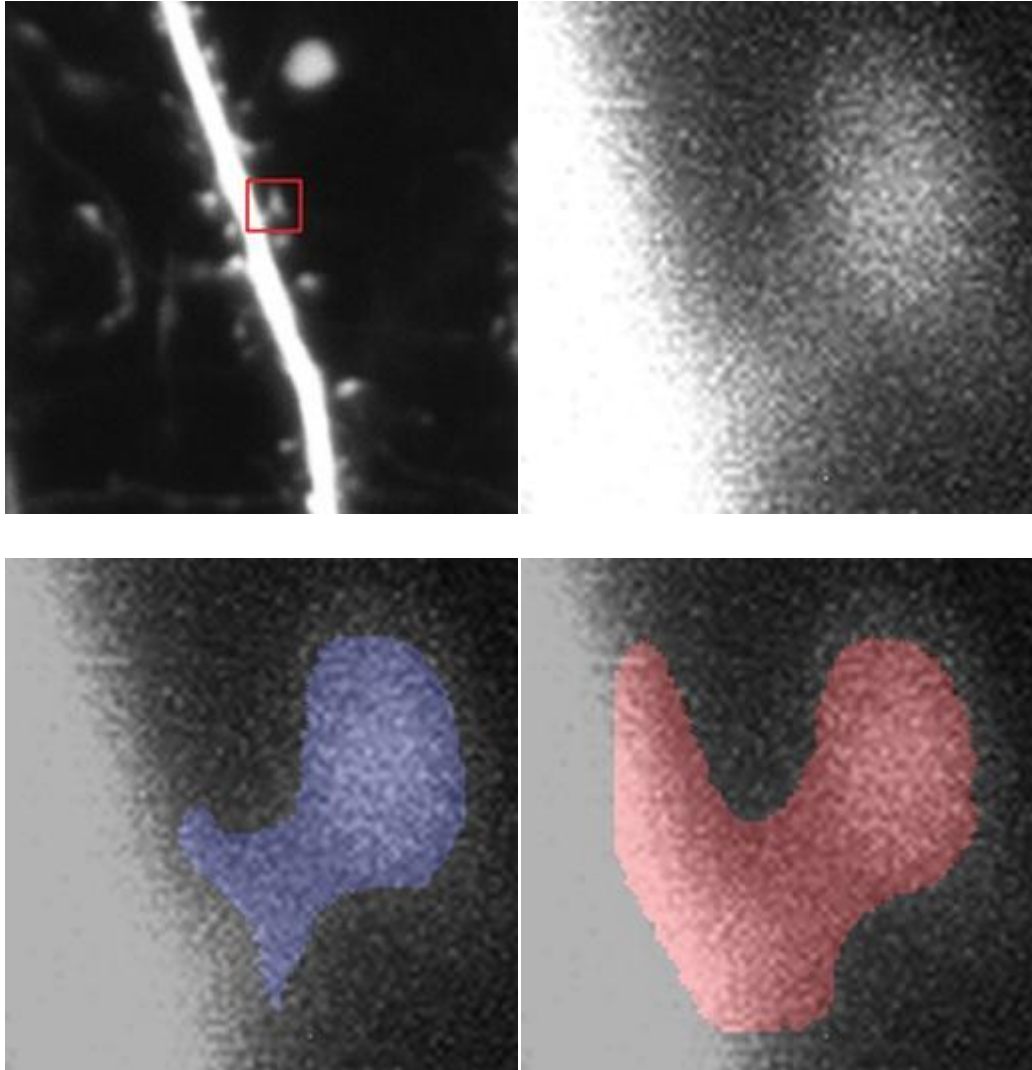


Figure 4.4: Exemplary segmentation with Active Contour of Spine 5 (Dice score=0.57). Blue corresponds manual segmentation and red represents automated segmentation.



This method results in higher Dice scores if the difference between the intensities (contrast) of spine head and neck are high. In that case active contour will evolve only to the head part and will achieve segmentation of the spine head only. Otherwise, it will act similar to the global thresholding and the success of segmentation will depend on ROI selection.

4.4 RESULTS OF ACTIVE CONTOUR WITH SHAPE PRIOR BASED SEGMENTATION

Active Contour with Shape Prior algorithm achieves higher Dice score for the segmentation of dendritic spines. Mean value of dice scores is 0.775 and the standard

deviation is 0.105. Exemplary results of Active Contour with Shape Prior method are given in Figures (4.5) and (4.6). The superiority of this method over the global thresholding and the active contour is the shape knowledge that limits the evolution of active contour. This property decreases the dependency of segmentation on the ROI selection and the intensity difference between spine head and neck.

Figure 4.5: Exemplary segmentation using Active Contour with Shape Prior on Grayscale image of Spine 1 (Dice score=0.84). Blue corresponds manual segmentation and red represents automated segmentation.

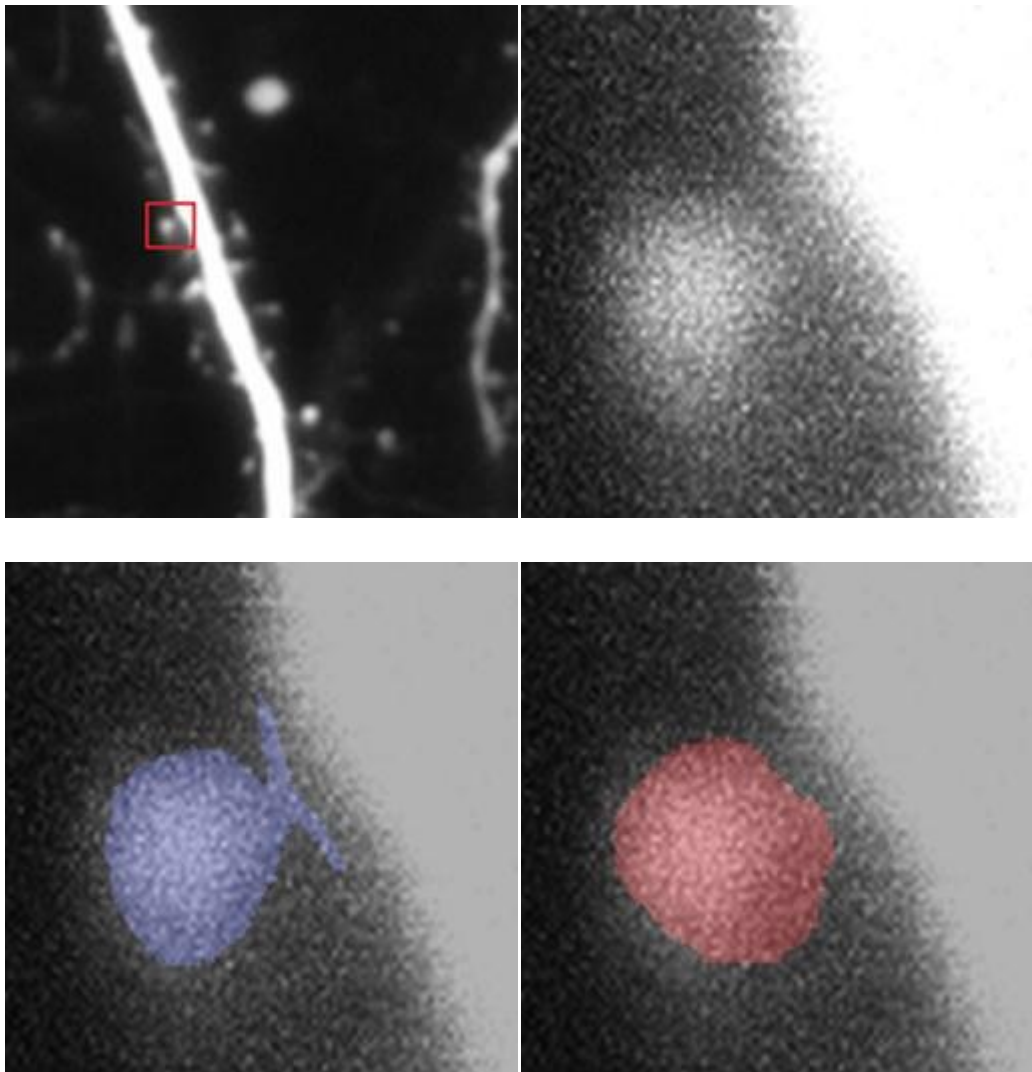
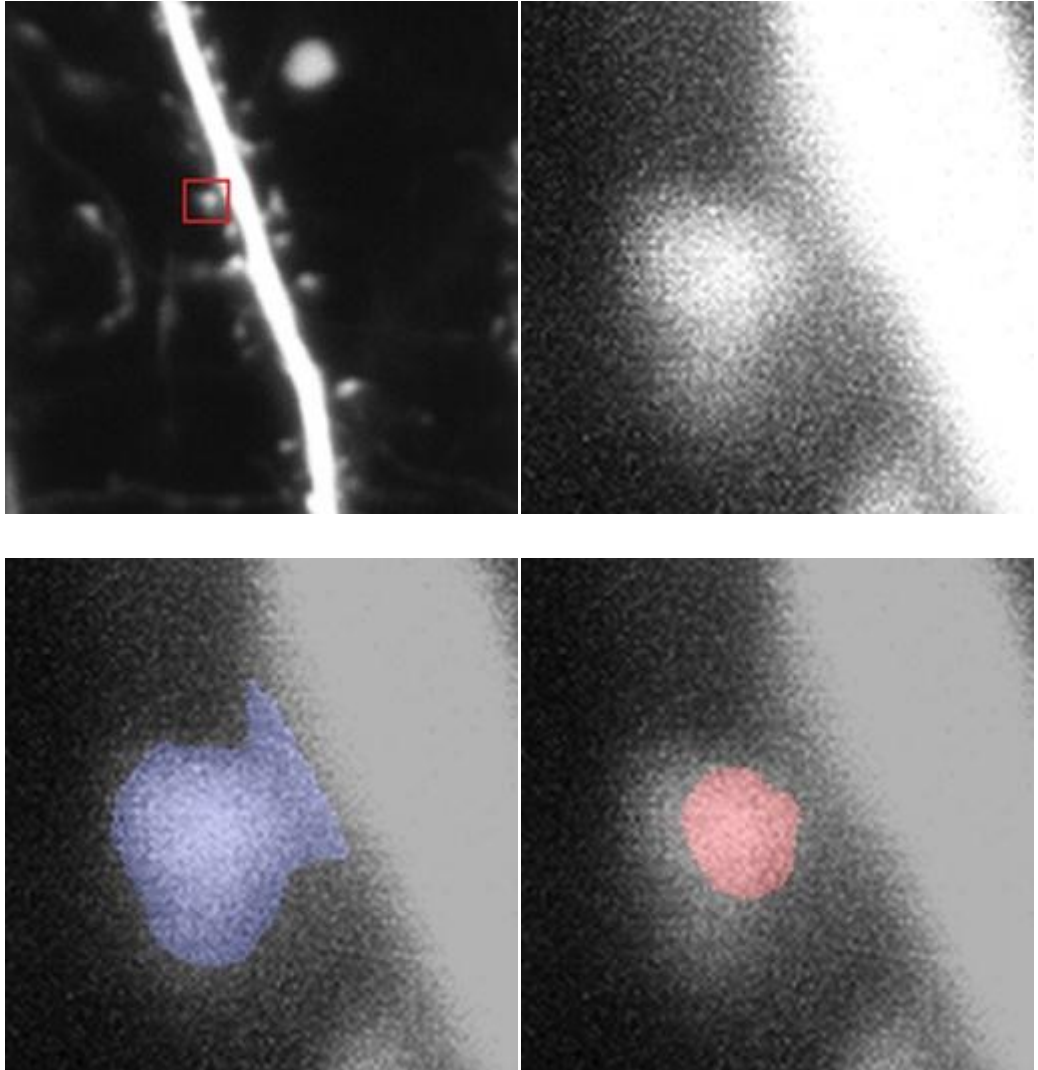
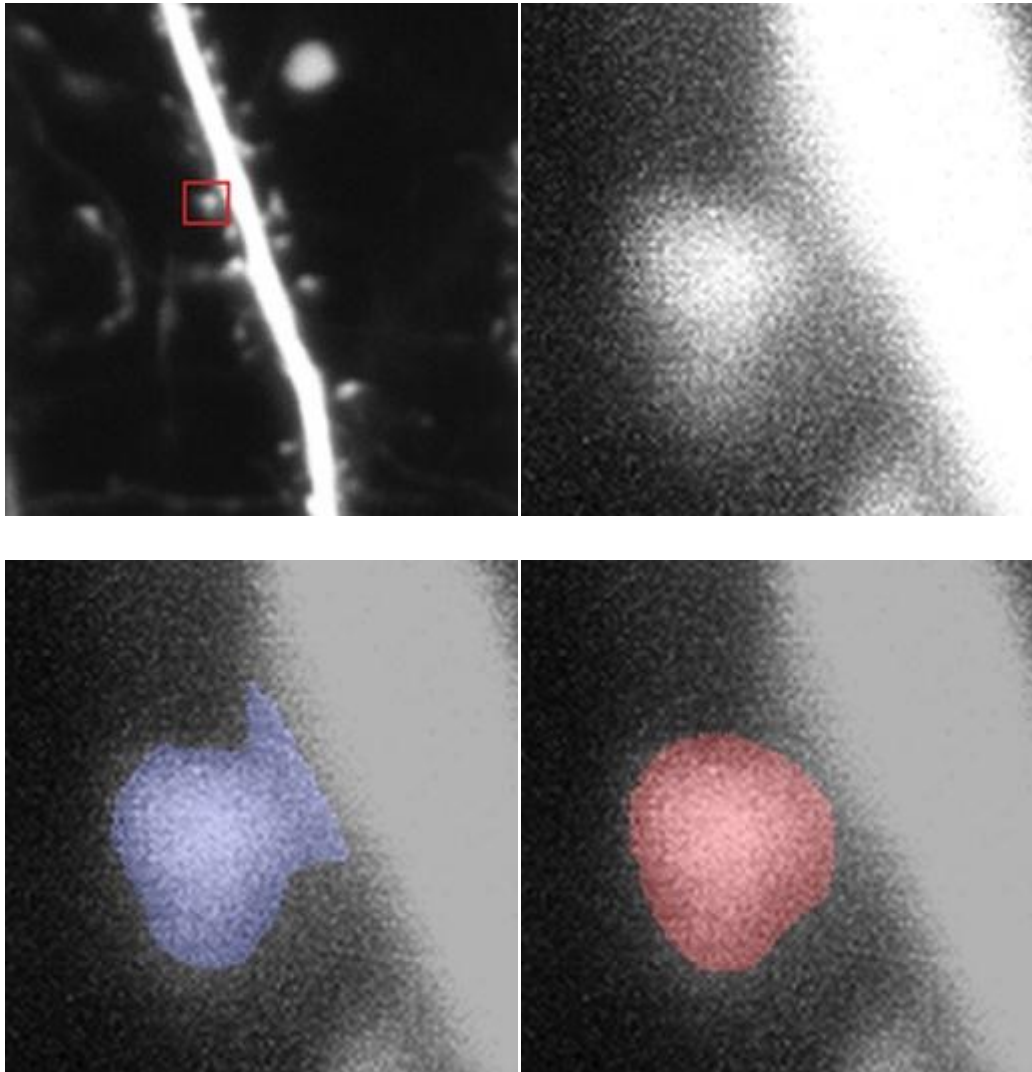


Figure 4.6: Exemplary segmentation using Active Contour with Shape Prior on Grayscale image of Spine 4 (Dice score=0.46). Blue corresponds manual segmentation and red represents automated segmentation.



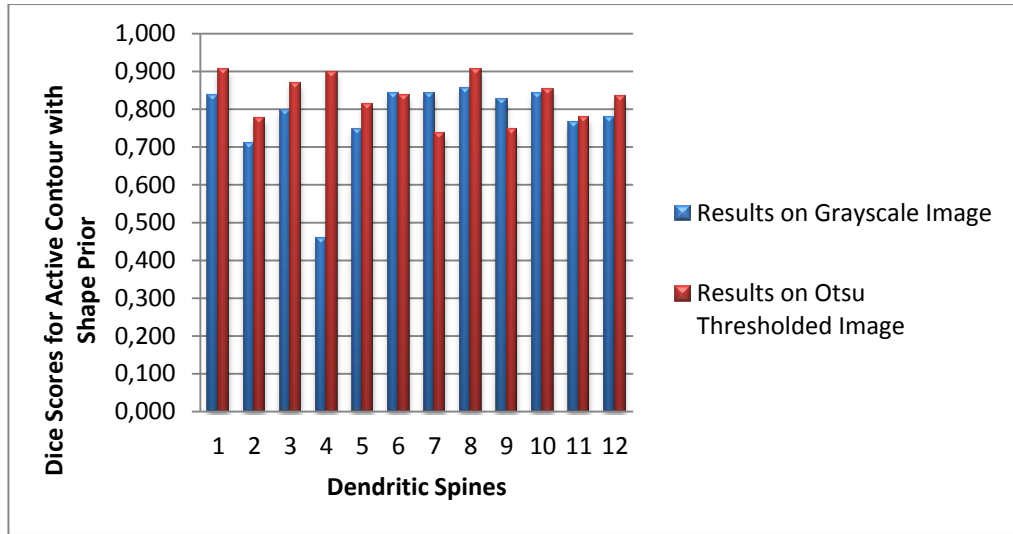
But in some cases initial active contour fits on the wrong intensity region and results in worse segmentation. In order to overcome this problem, this technique is applied on the Otsu Thresholded images instead of original grayscale images. The mean and standard deviation for the Dice scores of Active Contour with Shape Prior based segmentation are measured as 0.829 and 0.057, respectively. Visual result of Active Contour with Shape Prior based segmentation on Otsu Thresholded image can be seen in Figure (4.7).

Figure 4.7: Exemplary segmentation using Active Contour with Shape Prior on Otsu thresholded image of Spine 4 (Dice score=0.89). Blue corresponds manual segmentation and red represents automated segmentation.



In Figure (4.8) comparison between Active Contour with Shape Prior method on both grayscale and Otsu thresholded images are given. As it can be seen from the plot, results obtained using Otsu thresholded images are better in almost all cases.

Figure 4.8: Dice scores of Active Contour with Shape Prior.



In Table (4.3), Dice scores obtained by using Active Contour with Shape Prior, Active Contour and Global Thresholding based methods for spines 1 to 12 are given.

Table 4.3: Segmentation results for spine number 1-12 (S denotes Spine).

	Dice Score											
	S1	S2	S3	S4	S5	S6	S7	S8	S9	S10	S11	S12
Global (Otsu) Thresholding	0,54	0,22	0,55	0,68	0,58	0,58	0,63	0,91	0,89	0,80	0,92	0,86
Active Contour	0,74	0,81	0,70	0,66	0,57	0,65	0,72	0,90	0,94	0,78	0,90	0,87
Active Contour with Shape Prior using Grayscale Image	0,84	0,71	0,80	0,46	0,75	0,84	0,84	0,86	0,83	0,84	0,76	0,78
Active Contour with Shape Prior using Otsu Thresholded Image	0,91	0,78	0,87	0,90	0,81	0,84	0,74	0,90	0,75	0,85	0,78	0,83

Table 4.4 displays the mean and standard deviation for the Dice scores of each algorithm, where Active Contour with Shape Prior gives the higher Dice score result for dendritic spine segmentation.

Table 4.4: Dendritic spine segmentation results on the overall data set.

	Dice Score	
	Mean Value	Standard Deviation
Global (Otsu) Thresholding	0,68	0,20
Active Contour	0,77	0,11
Active Contour with Shape Prior using Grayscale Image	0,78	0,10
Active Contour with Shape Prior using Otsu Thresholded Image	0,83	0,06

Finally, for statistical significance analysis paired T-test is applied on the segmentation results. Our analysis revealed that the differences between the results of Global Thresholding as compared to the results of both Active Contour and Active Contour with Shape Prior are statistically significant (p -value <0.05). In the case of Active Contour versus Active Contour with Shape Prior, statistical significance of the results are found to be slightly less (p -value=0.09).

4.5 EFFECT OF ROI SELECTION

In order to evaluate the effect of ROI selection on the accuracy of the proposed algorithm for dendritic spine segmentation, several tests are applied on three dendritic spine images. In these tests, the location, size and orientation (angle of in-plane rotation) of the manually selected ROI are varied.

Figure 4.9 presents the results of the horizontal shift. As the degree of misplacement of the ROI (percentage shift in the graphical representation) increases, we observe a decrease in the mean Dice scores and an increase in the corresponding standard

deviations. The slightly asymmetric distribution observed relative to the vertical axis (no shift) can be attributed to the human error in the placement of the ROI by the expert. As it can be seen from the table, more than $\pm 20\%$ shift of manually selected ROI results in considerable drop in the Dice scores.

Figure 4.9: Effect of the horizontal shift of the manually selected ROI on the segmentation accuracy. Horizontal axis represents the percentage shift relative to the horizontal size of the ROI (“-” values show left-shift); whereas, vertical axis corresponds to the Dice score. Blue markers represent the mean values, while the corresponding error bars depict standard deviations.

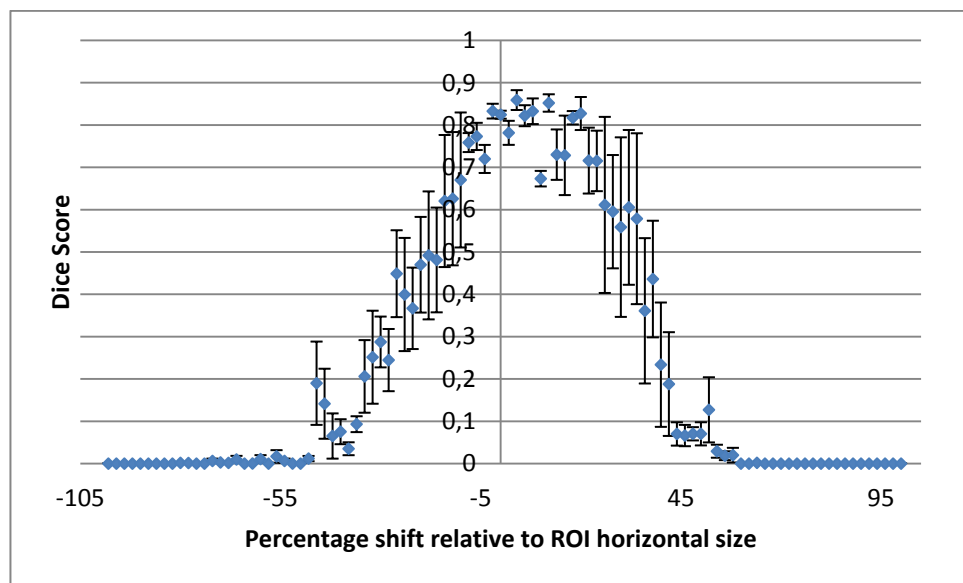


Figure 4.10 shows the effect of vertical shift in the ROI placement on the segmentation accuracy, where results similar to those of the horizontal shift test are observed. In the $\pm 20\%$ shift range this operation results with higher dice score and lower standard deviation which are close to the result of manual ROI selection. On the other hand, if the percentage of shift operation is more than $\pm 20\%$, dice score starts to decline dramatically.

Figure 4.10: Effect of vertical shift of manually selected ROI to the segmentation accuracy. Horizontal axis represents the percentage shift relative to the vertical size of the ROI (“-” values show up-shift); whereas, vertical axis corresponds to the Dice score. Blue markers represent the mean values, while the corresponding error bars depict standard deviations.

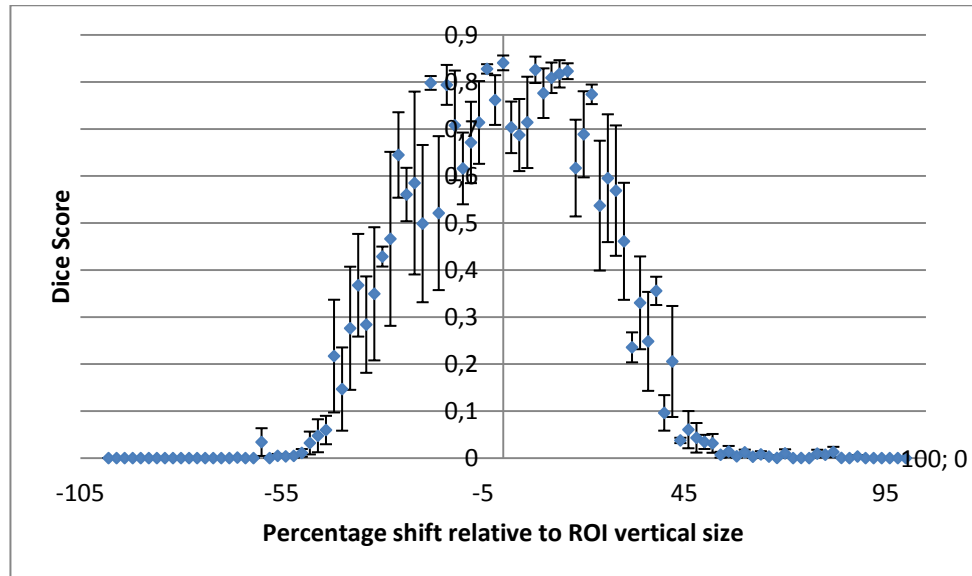
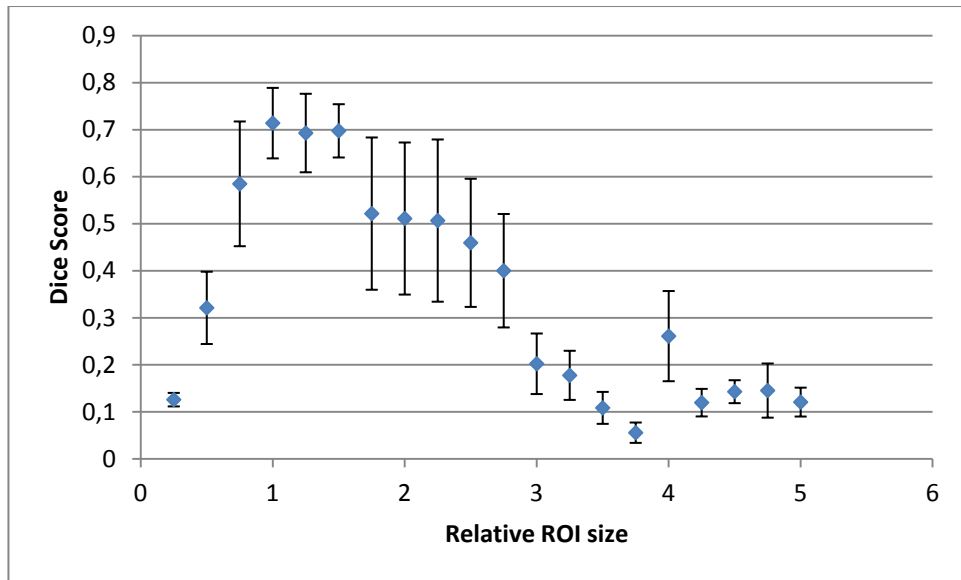


Figure 4.11 displays the effect of ROI size on the segmentation accuracy. For this test, ROIs with varying sizes (scales) are always placed at the center of the spine head, so that at all scales it is guaranteed that the resulting ROI will contain some part of the spine head. Tested scales ranges from 0.25 to 5 with steps of 0.25. As observed, selection of ROI size is crucial to obtain accurate segmentations. It is observed that for the medium scales (0.75-1.75) this effect is minimal, while for the lower and higher extremes (scales below 0.75 and above 1.75) the segmentation accuracy is dramatically decreased. This is due to the fact that at lower scales the ROI covers the spine head only partially, while at higher scales dendrite regions are also included in the ROI and thus false segmentations occur.

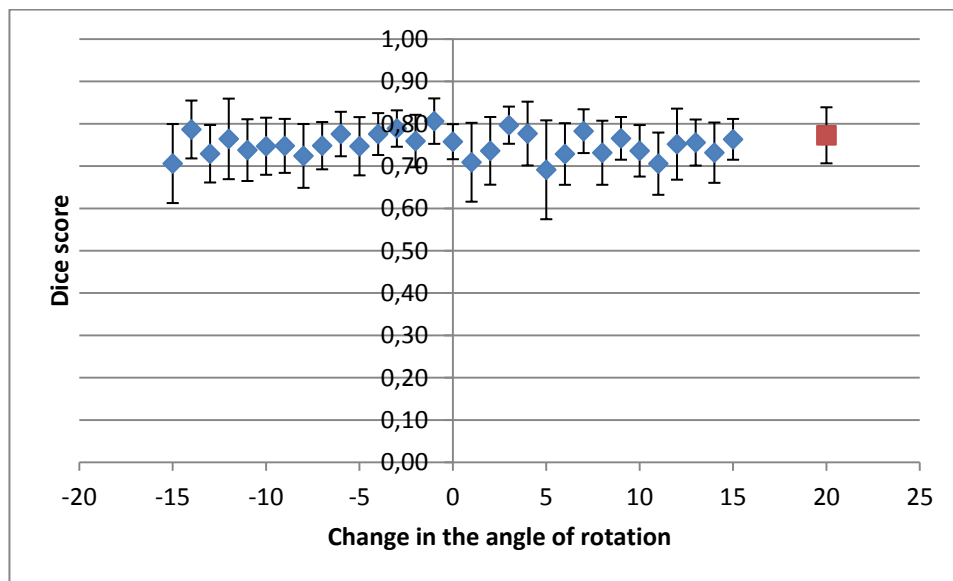
Figure 4.11: Effect of ROI size on the segmentation accuracy.



Dendritic spines in our training set (Figure 3.4) are oriented to the right, but the spines that we want to segment can be orientated in any direction. Therefore, there needs to be a rotation operation applied prior to the segmentation stage. Our segmentation method is capable of applying rotation via geometric transformations, but it is inadequate for accurate dendritic spine segmentation as a result of limited information provided by the training set. Our training set contains only the spine head and a small portion of the spine neck; it does not contain any information from the dendrite part. This lack of information cannot be sufficient to detect the exact orientation of the dendritic spine in a given ROI, and therefore leads to erroneous detection of orientation and low accuracy in segmentation. In order to overcome this problem, we define two solutions; (i) iterative segmentation using the active contour with shape prior method, and (ii) semi-automated rotation prior to segmentation. In the first solution, we will use two different training sets; first one will contain some portions of the dendrite, spine neck and spine head, and the other set will be the same as our current training set (containing only head and neck portions of the spines). In this iterative method, first we will run segmentation using the first training set, then employ the second training set and extract spine head from the result of the first segmentation. In the second method, a semi-automated rotation is applied to the selected ROI by the user before the segmentation is realized. This semi-automated method calculates the minor and major axis of the selected ROI and then calculates an angle that will rotate the major axis as it will be parallel to x-axis. But this

method does not guarantee that spine head will be right-oriented, it just guarantees that it will be on the horizontal axis. Therefore, a manual interaction that corrects the orientation is used. In this study we employed the second alternative for spine orientation since the first alternative requires relatively more run time. Therefore, we apply a rotation operation to the selected ROI before segmentation. In order to analyze the effect of this rotation operation, a test is prepared. According to this test a rotation angle is calculated with the semi-automated method and then segmentation algorithm applied to the ROI rotated in the range of ± 15 to that angle. This test is applied on 14 different dendritic spines and in Figure 4.12 results of this test can be seen. As it can be seen from the graph, ± 15 degree angle variation results in similar accuracies as compared to both the semi-automated and manual approaches.

Figure 4.12: Effect of ROI rotation on the segmentation accuracy. Blue markers represent the mean result of segmentation in the range of ± 15 to the angle found with semi-automated method. Red marker refers to the result of the expert's manual ROI selection.



5. DISCUSSIONS AND RESULTS

5.1 RESULTS

Dendritic spine analysis is one of the most important research areas of Neuroscience since the morphological and statistical properties, such as number, length and volume of dendritic spines, can play a role in learning process or can be used for understanding the reasons and effects of mental disorders (Choy et al., 2010). But manual analysis of dendritic spines is hard and time-consuming since there is a vast amount of data thanks to the advancements in imaging technology. Therefore, these analyses should be done by using automated tools. The automated tools should detect dendritic spines, segment them properly and make a post-analysis for calculating the statistical properties of dendritic spines and monitoring the related changes.

In this thesis we worked on a specific part of dendritic spine analysis problem, namely dendritic spine segmentation, which will be a part of an automated tool that will analyze and track statistical properties of dendritic spines (e.g. measuring and tracking volume of a dendritic spine). Since head part of the spine is used for these analyses, our segmentation will also focus on the head part. The accuracy of such analyses is directly connected to the accuracy of segmentation. Therefore, automated segmentation results must be close to the manual segmentations of the experts.

We propose the use of Active Contour with Shape Prior method of Bresson et al. (2006) for the segmentation of dendritic spines. In this method, evolution of active contours is controlled with energy minimization function solved using three terms: shape, boundary and region. Boundary term is the result of image gradients, region term is calculated using the intensity values in the segmented region via Mumford-Shah function, and shape term is calculated according to the shape knowledge obtained from a training set.

This method is applied on preprocessed dendritic spine images via median filtering and its results are compared with two other methods; (1) Global thresholding (or Otsu Thresholding), and (2) Active Contour method proposed by Chan and Vese (2001).

Median filtering was selected for noise reduction. In the early stages of this study size of median filter was used, ranging from 3x3 to 19x19. According to the mean Dice score values and the standard deviations obtained with these filter sizes, 11x11 were selected as the final filter size thanks to its higher Dice score and lower standard deviation.

Among the three segmentation methods used Otsu thresholding based one has resulted in the lowest dice score, since this method is not able to separate the spines from the dendrite within the selected region of interest (ROI). Nevertheless in some cases the Dice score for Otsu thresholding based dendritic spine segmentation can be as high as 0.91 (Figure 4.2), which can be attributed to the ROI selection step. If the selected ROI contains only spine, then the segmentation will be more accurate. However such ROI selection is very difficult to achieve (even for expert users) since in most cases dendrite and spines are very close to each other and it is hard to leave out the dendrite from the ROI.

Active contour based spine segmentation generally results in better segmentations in comparison to the use of Otsu thresholding. Our observations reveal that active contour method is superior to Otsu thresholding especially on the spines that are not touching the dendrite. In such cases active contour will evolve only in the spine region and will not be affected by the dendrite (Figure 4.3). In the case of touching spines active contour approach, similar to Otsu thresholding, cannot separate spines from the dendrite and therefore yields lower Dice scores (Figure 4.4).

Active Contour with Shape Prior algorithm achieves higher Dice scores for the segmentation of dendritic spines. This algorithm can separate spines from dendrite even for the touching cases thanks to the shape prior guiding the curve evolution. However, in some cases this algorithm may also lead to bad results, due to the low tissue contrast in the original images. Dendrite images are grayscale images that contain several intensity regions. These intensity regions are very close to each other and if the initial curve fits on a wrong intensity region then the curve will evolve towards wrong directions. As a result, segmentation will end up with a low dice score. An example of such segmentation can be seen in Figure 4.6. In order to overcome this issue we propose to run this algorithm on the Otsu thresholded image rather than on the original grayscale

image. By this way, the contrast variation is minimized and the resulting curve evolution becomes more robust. Using this algorithm on Otsu thresholded binary images has increased the average Dice from 0.78 to 0.83 and the standard deviation has decreased from 0.11 to 0.06. Figure 4.7 is an exemplary segmentation result obtained by applying Active Contour with Shape Prior method on Otsu thresholded image of Spine 4 and the Dice score is 0.90. On the other hand, applying Active Contour with Shape Prior method on grayscale image of Spine 4 is resulted with the Dice score of 0.46.

Experimental results indicate that active contour with shape prior (initialized with a binary input instead of the original grayscale image) results in better segmentation accuracy as compared to global thresholding and active contour methods.

One of the most important steps of this segmentation method is the ROI selection, which is realized such that the spine head falls approximately to the center of the ROI where the initial curve will be placed. In order to analyze the effect of ROI selection on segmentation accuracy, several tests were applied by changing location, size and orientation (angle of in-plane rotation) of the manually selected ROI. According to the results of location variation, mean Dice scores decrease and corresponding standard deviations increase as the misplacement of ROI increases. Up to 20% change in the placement of ROI (shift to left, right, up or down) relative to its size can be acceptable. The size of ROI is varied with different scale factors in order to check its effect on segmentation. Results suggest that scale factors between 0.75 and 1.75 give similar accuracies. Whereas factors below 0.75 results in lower accuracy since these ROIs only contain limited part of spine head, and factors above 1.75 result in inaccurate segmentation since they contain larger amount of dendrite region in the ROI.

Segmentation accuracy of the proposed method depends on the orientation of the spine. This spine has to be oriented in the same direction as the spines in the training set. Although the proposed active contour with shape prior method can intrinsically perform orientation via geometric transformations, but our observations showed that this orientation fails to be adequate due to the limited shape information provided by the training set. Therefore, a rotation process is applied to the selected ROI before segmentation and a semi-automated method is used to find the angle of rotation. Effect of this angle to the segmentation accuracy is tested by varying the angle in the ± 15

degree range. According to the results, angle change in this range gives similar accuracies. As a result, finding the rotation angle with a sensitivity of ± 15 degrees is regarded as adequate for better segmentation with the proposed method.

5.2 FUTURE WORKS

In the present work, accuracy of the active contour with shape prior approach depends on the orientation of the input spine with respect to the training shapes. To this end, prior to segmentation spines were rotated to the desired orientation manually or via semi-automated method explained in Section 4.5 in this thesis. In order to make this segmentation method fully automated, a solution that rotates the dendritic spines in the proper direction has to be provided.

Current results for dendritic spine segmentation are obtained using spines with circular shapes since these types of spines are mostly selected for statistical analyses by the experts. However, spines with different shapes, like mushroom, should be segmented as well. Therefore, training sets for different shapes of dendritic spines can be created and the Active Contour with Shape Prior method can be applied on such spines.

From this thesis, a paper named *Dendritic Spine Segmentation Using Active Contour with Shape Prior* (Akarsu et al. 2012) is accepted to MASFOR 2012 Conference organized by The Department of Electrical & Electronics Engineering of Bogazici University, Istanbul, Turkey. We are also planning to submit another publication summarizing the results of this work to an IEEE Journal in the near future.

REFERENCES

Books

Hearn D, Baker MP., 1996. *Computer Graphics*. New Jersey: Prentice Hall.

Purves, D., Augustine, G.J., Fitzpatrick, D., Hall, W.C., Lamantia, A., McNamara, J.O.,
White, L.E., 2008. *Neuroscience*. Sinauer Associates, Inc.

Ramon y Cajal, S., 1995. *Histology of the Nervous System of Man and Vertebrate*.
Oxford University Press.

Valeur, B., 2001. *Molecular Fluorescence: Principles and Applications*. Wiley-VCH.

Periodicals

- Adalsteinsson, D. and Sethian, J., 1995. A fast level set method for propagating interfaces. *Journal of Computational Physics*. **118**, pp. 269–277.
- Bai, W., Zhou, X., Ji, L., Cheng, J., and Wong, S. T. C., 2007. Automatic dendritic spine analysis in two-photon laser scanning microscopy images. *Cytometry Part A*. **71A**(10), pp. 818–826.
- Bear, M.F., Huber, K.M., Warren, S.T., 2004. The mGluR theory of fragile X mental retardation. *Trends in Neurosciences*. **27**(7), pp. 370-377.
- Bresson, X., Vandergheynst, P., Thiran, J. , 2006. A Variational Model for Object Segmentation Using Boundary Information and Shape Prior Driven by the Mumford-Shah Functional. *International Journal of Computer Vision*. **68**(2), pp. 145–162.
- Cheng, J., Zhou, X., Miller, E., Witt, R. M., Zhu, J., Sabatini B.L., Wong, S.T.C. , 2007. A novel computational approach for automatic dendrite spines detection in two-photon laser scan microscopy. *Journal of Neuroscience Methods*. **166**, pp. 122–134.
- Coss, R.G. and Perkel, D.H., 1985. The function of dendritic spines: a review of theoretical issues. *Behavioral and Neural Biology*. **44**, pp. 151–185.
- Denk, W., Strickler, J.H. and Webb, W.W., 1990. Two-photon laser scanning fluorescence microscopy. *Science*. **248**(4951), pp. 73-76.
- Govindarajan, A., Israely, I., Huang, S. & Tonegawa, S., 2011. The dendritic branch is the preferred integrative unit for protein synthesis-dependent LTP. *Neuron*.
- Göppert-Mayer, M., 1931. Über Elementarakte mit zwei Quantensprüngen. *Ann Phys*. **9**, pp. 273-295.
- Greenough, W.T. and Bailey, C.H., 1988. The anatomy of a memory: convergence of results across a diversity of tests. *Trends in Neurosciences*. **11**, pp. 142–147.

- Harvey C.D., Svoboda K., 2007. Locally dynamic synaptic learning rules in pyramidal neuron dendrites. *Nature*. **450**(7173), pp. 1195-1200.
- Janoos, F., Mosaliganti, K., Xu,X., Machiraju, R. , Huang, K. , Wong, S.T.C. , 2009. Robust 3D reconstruction and identification of dendritic spines from optical microscopy imaging. *Medical Image Analysis*. **13**, pp. 167–179.
- Kasai, H., Fukuda, M., Watanabe, S., Hayashi-Takagi, A., & Noguchi, J., 2010. Structural dynamics of dendritic spines in memory and cognition. *Trends in Neurosciences*. **33**(3), pp. 121-129.
- Leiss, F. et al., 2009. Characterization of dendritic spines in the Drosophila central nervous system. *Developmental Neurobiology*. **69**, pp. 221–234.
- Osher, S. and Sethian, J.A., 1988. Fronts propagating with curvature dependent speed: Algorithms based on Hamilton-Jacobi formulations. *Journal of Computational Physics*. **79**(1), pp. 2–49.
- Otsu, N., 1979. A threshold selection method from gray-level histograms. *IEEE Trans. Sys., Man*. **9**(1), pp. 62–66.
- Rodriguez, A., Ehlenberger, D.B., Dickstein, D.L., Hof, P.R. and Wearne, S.L., 2008. Automated Three-Dimensional Detection and Shape Classification of Dendritic Spines from Fluorescence Microscopy Images. *PLoS ONE*. **3**(4).
- Son, J., Song, S., Lee, S., Chang, S., Kim, M. , 2010. Morphological change tracking of dendritic spines based on structural features. *Journal of Microscopy*.
- Tanaka, J. et al., 2008. Protein Synthesis and Neurotrophin-Dependent Structural Plasticity of Single Dendritic Spines. *Science*. **319**, 1683.
- Unser, M., 1999. Splines: A perfect fit for signal and image processing. *IEEE Signal Processing Magazine*. **16**(6), pp. 22–38.
- Vese, L.A. and Chan, T.F., 2002. A multiphase level set framework for image segmentation using the Mumford and Shah model. *International Journal of Computer Vision*. **50**(3), pp.271– 293.

- Weaver, C.M., Hof, P.R., Wearne, S.L. and Lindquist, W.B., 2004. Automated algorithms for multiscale morphometry of neuronal dendrites. *Neural Computation*. **16**, pp. 1353- 1383.
- Zhang, Y. , Zhou, X., Witt, R. M., Sabatini, B. L., Adjeroh, D. &Wong, S. T. C., 2007. Dendritic spine detection using curvilinear structure detector and lda classifier. *NeuroImage*. **36**(2), pp. 346 - 360.
- Zhang, Y., Chen, K., Baron, M., Teylan, M. A., Kim, Y., Song, Z., Greengard, P. &Wong, S. T. C., 2010. A neurocomputational method for fully automated 3D dendritic spine detection and segmentation of medium-sized spiny neurons. *NeuroImage*. **50**(2010), pp. 1472 - 1484.

Other Sources

- Akarsu, C., Ünay, D., Argunşah, A. Ö., Ramiro-Cortés, Y., Hobbiss A. F., Israely, I., 2012. Dendritic Spine Segmentation Using Active Contour With Shape Prior. *MASFOR*.
- Choy, S., Chen, K., Zhang, Y., Baron, M., Teylan, M. A., Kim, Y., Tong, C., Song, Z., Wong, S.T.C., 2010. Multi Scale and Slice-based Approach for Automatic Spine Detection. *Annual International Conference of the IEEE EMBS*.
- Luisier, F., Vonesch, C., Blu, T., Unser, M., 2009. Fast Haar-wavelet denoising of multidimensional fluorescence microscopy data. *Biomedical Imaging: From Nano to Macro, 2009. ISBI '09. IEEE International Symposium on*. pp.310-313.

CURRICULUM VITAE

Name Surname: Cemal Akarsu

Address: Hurriyet M. Kuloglu S. No:23 / 11 Bahcelievler / Istanbul

Date and Place of Birth: Istanbul - 28.05.1986

Foreign Language: English

Elementary Education: Kuleli Elementary School, 1997

Secondary Education: Fahrettin Kerim Gokay Anatolian High School, 2001
Kultur Science High School, 2004

Undergraduate Education: Sabanci University, 2009

Graduate Education: Bahcesehir University, Present

Name of Institute: Graduate School Of Natural And Applied Sciences

Name of Program: Electrical and Electronics Engineering

Paper: Dendritic Spine Segmentation Using Active Contour with Shape Prior,
MASFOR 2012 Conference

Work Experience:

- TÜBİTAK UEKAE – Researcher – 2010- 2012
- STEricsson – Digital Design Engineer at FPGA Team – 2009- 2010